REFERENCES

Elliott CE, Becker B, Oehler S, Castanon MJ, Hauptmann R, Wiche G (1997) Plectin transcript diversity: identification and tissue distribution of variants with distinct first coding exons and rodless isoforms. *Genomics* 42:115–25

Fine JD, Eady RA, Bauer EA, Briggaman RA, Bruckner-Tuderman L, Christiano A *et al.* (2000) Revised classification system for inherited epidermolysis bullosa: Report of the Second International Consensus Meeting on diagnosis and classification of epidermolysis bullosa. *J Am Acad Dermatol* 42:1051–66

Fuchs P, Zorer M, Rezniczek GA, Spazierer D, Oehler S, Castanon *et al.* (1999) Unusual 5′ transcript complexity of plectin isoforms: novel tissue-specific exons modulate actin binding activity. *Hum Mol Genet* 8:2461–72

Litjens SH, de Pereda JM, Sonnenberg A. (2006) Current insights into the formation and breakdown of hemidesmosomes. *Trends Cell Biol* 16:376–83

Liu CG, Maercker C, Castanon MJ, Hauptmann R, Wiche G (1996) Human plectin: organization of the gene, sequence analysis, and chromosome localization (8q24). *Proc Natl Acad Sci USA* 93:4278–83

McLean WH, Pulkkinen L, Smith FJ, Rugg EL, Lane EB, Bullric F *et al.* (1996) Loss of plectin causes epidermolysis bullosa with muscular dystrophy; cDNA cloning and genomic organization. *Genes Dev* 10:1724–35

McMillan JR, Akiyama M, Rouan F, Mellerio JE, Lane EB, Leigh IM *et al.* (2007) Plectin defects in epidermolysis bullosa simplex with muscular dystrophy. *Muscle Nerve* 35:24–35

Nakamura H, Sawamura D, Goto M, Nakamura H, McMillan JR, Park S *et al.* (2005) Epidermolysis bullosa simplex associated with pyloric atresia is a novel clinical subtype caused by mutations in the plectin gene (*PLEC1*). *J Mol Diagn* 7:28–35

Pulkkinen L, Uitto J (1999) Mutations analysis and molecular genetics of epidermolysis bullosa. *Matrix Biol* 18:29–42

Pfendner E, Rouan F, Uitto J (2005a) Progress in epidermolysis bullosa: the phenotypic spectrum of plectin mutations. *Exp Dermatol* 14:241–9

Pfendner E, Uitto J (2005b) Plectin gene mutations can cause epidermolysis bullosa with pyloric atresia. *J Invest Dermatol* 124:111–5

Rezniczek GA, Abrahamsberg C, Fuchs P, Spazierer D, Wiche G (2003) Plectin 5′-transcript diversity: short alternative sequences determine stability of gene products, initiation of translation and subcellular localization of isoforms. *Hum Mol Genet* 12: 3181–94

Shimizu H, Takizawa Y, Pulkkinen L, Murata S, Kawai M, Hachisuka H *et al.* (1999) Epidermolysis bullosa simplex associated with muscular dystrophy phenotype-genotype correlation and review of the literature. *J Am Acad Deramtol* 41:950–6

Smith FJ, Eady RA, Leigh IM, McMillan JR, Rugg EL, Kelsell DP *et al.* (1996) Plectin deficiency results in muscular dystrophy with epidermolysis bullosa. *Nat Genet* 13:450–7

Steinboeck F, Kristufek D (2005) Identification of the cytolinker protein plectin in neuronal cellst – expression of a rodless isoform in neurons of the rat superior cervical ganglion. *Cell Mol Neurobiol* 25:1151–69

Wiche G (1998) Role of plectin in cytoskeleton organization and dynamics. *J Cell Sci* 111:2477–86

A Novel *GJB2* Mutation p.Asn54His in a Patient with Palmoplantar Keratoderma, Sensorineural Hearing Loss and Knuckle Pads

Journal of Investigative Dermatology (2007) **127,** 1540–1543. doi:10.1038/sj.jid.5700711; published online 25 January 2007

TO THE EDITOR

Mutations in the *GJB2* gene encoding connexin26 are the major cause of autosomal-recessive or -dominant non-syndromic congenital sensorineural hearing loss (SNHL) (Kelsell *et al.*, 1997; Kenneson *et al.*, 2002; refer to the connexin-deafness homepage at http://davinci.crg.es/deafness/). In addition, connexin26 mutations have been identified in autosomal-dominant syndromic congenital SNHL with palmoplantar keratoderma (PPK) (Maestrini *et al.*, 1999; Richard *et al.*, 2002, 2004; Brown *et al.*, 2003; van Steensel *et al.*, 2004; Arita *et al.*, 2006). We have encountered a Japanese boy with PPK, knuckle pads and congenital SNHL and *GJB2* mutation analysis revealed a novel mutation p.Asn54His.

The patient was a 12-year-old Japanese boy with PPK, knuckle pads on the fingers and severe SNHL. He had a congenital onset of profound bilateral SNHL. At 1 year of age, he developed PPK and knuckle pads. There was no familial history of skin disorders or auditory dysfunction. At age 12, moderate PPK was seen. Knuckle pads were apparent on all his fingers (Figure 1a and b). Acneiform follicular keratotic papules were seen on his forehead and face, although these acneiform papules might just be acne. No mutilation (pseudoainhum) was seen on the fingers. Nails, hair, and teeth were normal and no leukonychia was observed. Ophthalmologic examination revealed no apparent abnormality.

Abbreviations: PPK, palmoplantar keratoderma; SNHL, sensorineural hearing loss

The medical ethical committee at Hokkaido University approved all studies described below. The study was conducted according to the Declaration of Helsinki Principles. Participants or their legal guardian gave their written informed consent. The coding region of *GJB2* (Genbank accession no. NM 004004) was amplified from genomic DNA by PCR, as described previously (Richard *et al.*, 1998). Direct sequencing of the patient's PCR products revealed that the patient was a heterozygote for a novel missense mutation p.Asn54His (A to C substitution at nucleotide position 160: asparagine 54 (AAC) to histidine (CAC)) in *GJB2* (Figure 1d), which was not found in his mother. We were unable to obtain a DNA sample from his father. This mutation was not found in 100 normal unrelated Japanese alleles

DOI:10.1111/j.1600-0625.2007.00614.x
www.blackwellpublishing.com/EXD

Original Article

Localization of ABCA12 from Golgi apparatus to lamellar granules in human upper epidermal keratinocytes

Kaori Sakai, Masashi Akiyama, Yoriko Sugiyama-Nakagiri, James R. McMillan, Daisuke Sawamura and Hiroshi Shimizu

Department of Dermatology, Hokkaido University Graduate School of Medicine, N15 W7, Sapporo 060-8638, Japan
Correspondence: Masashi Akiyama, MD, PhD, Department of Dermatology, Hokkaido University Graduate School of Medicine, N15 W 7, Sapporo 60-8638, Japan, Tel.: +81-11-716-1161, ext. 5962, Fax: +81-11-706-7820, e-mail: akiyama@med.hokudai.ac.jp

Accepted for publication 11 July 2007

Abstract: ABCA12 is an ATP-binding cassette transporter and is thought to act as a transmembrane lipid transporter. We reported that deleterious ABCA12 mutations cause a disturbance in lamellar granule (LG) lipid transport in the epidermal granular layer keratinocytes, resulting in harlequin ichthyosis, a severe genodermatosis. Detailed localization of ABCA12 in comparison with glucosylceramide and Golgi apparatus markers were studied in order to obtain clues to clarify the function(s) of ABCA12 in human skin. We performed double-labelling immunofluorescent staining using antibodies against ABCA12, glucosylceramide and two Golgi apparatus markers (TGN46 and GM130) in normal human skin and cultured keratinocytes. Immunogold electron microscopy for *ABCA12* and glucosylceramide was studied on postembedding and cryoultrathin sections of normal human skin. Confocal laser scanning microscopy demonstrated that ABCA12 and glucosylceramide co-localized in the granular layer keratinocytes as well as in keratinocytes cultured in high Ca^{2+} conditions through the Golgi apparatus to the cell periphery. Postembedding immunogold electron microscopy revealed that both ABCA12 and glucosylceramide labellings were associated with the LG of the uppermost granular layer keratinocytes. Using cryoultramicrotomy, lamellar structures in the LG were more clearly observed, and ultrastructural localization of *ABCA12* and glucosylceramide was better demonstrated to LG in the uppermost granular layer cells. These results indicate that *ABCA12* plays an important role in lipid transport from the Golgi apparatus to LG in human granular layer keratinocytes.

Key words: ATP – keratinization – lipid barrier – secretion – trafficking

Please cite this paper as: Localization of ABCA12 from Golgi apparatus to lamellar granules in human upper epidermal keratinocytes. Experimental Dermatology 2007; 16: 920–926.

Introduction

The ATP-binding cassette (ABC) transporter superfamily is one of the largest gene families, encoding highly conserved proteins involved in energy-dependent transport of a variety of substrates across membranes, including ions, amino acids, peptides, carbohydrates, and lipids (1–4). The 48 currently known ABC genes are classified into seven subfamilies, based on sequence homology and organization of their nucleotide-binding folds. ABC genes are widely dispersed throughout the eukaryotic genome and are highly conserved between species (5). The ABCA subfamily, of which the ABCA12 gene is a member, comprises 12 full transporters and one pseudogene (*ABCA11*) and is thought to work in lipid transport (5). Among the several subclasses of ABC transporters, the ABCA subclass (6) has received considerable attention because of four ABCA genes in the subfamily: *ABCA1*, *ABCA3*, *ABCA4* and *ABCA12* that have been implicated in the development of genetic diseases affecting lipid transport (7,8). ABCA1 is a defective protein underlying Tangier disease (MIM 205400), familial hypoalphalipoproteinemia (MIM 604091) and premature atherosclerosis (9–11). *ABCA4* mutations underlie Stargardt disease (MIM 248200), some forms of autosomal recessive retinitis pigmentosa (MIM 601718) and autosomal recessive cone–rod dystrophy (MIM 604116) and macular degeneration (MIM 153800) (11–13). Cholesterol/phospholipids and protonated *N*-retinylidene phosphatidylethanolamine were suggested to be substrates for *ABCA1* and *ABCA4*, respectively (14–17). *ABCA1* and *ABCA7* were reported to be expressed in the epidermal keratinocytes (18,19).

Extracellular lipid including ceramide is thought to be essential for skin barrier function (20). Mutations in the ABC transporter A12 gene (*ABCA12*) were reported to underlie the devastating phenotype seen in Harlequin ichthyosis (HI) patients (21,22), the most severe keratinization disorder thus far known. *ABCA12* mutations

Abbreviations: ABC, ATP-binding cassette; ABCA12, ABC transporter A12; LG, lamellar granule.

underlying HI are thought to lead to major disruptive defects in ABCA12 lipid transporter function resulting in the HI phenotype (21). Since 2005, a number of HI patients with ABCA12 mutations have been reported in the literature (23–28). We reported previously that ABCA12 is localized in lamellar granules (LG) in the granular layer keratinocytes and might work in the lipid transport via LG to form the intercellular lipid layers in the stratum corneum (21). However, the detailed pathomechanisms of abnormal lipid accumulation in the keratinocyte cytoplasm and defective lipid secretion from keratinocytes has not been completely clarified in HI. The aim of the present study was to clarify the precise localization sites of ABCA12 in epidermal keratinocytes *in vivo* and *in vitro* in comparison with other keratinization-associated molecules and Golgi apparatus-associated molecules, and to have clues to further characterize the detailed function of ABCA12 in keratinocyte lipid transport. We have analyzed the epidermal localization of ABCA12 in comparison with the localization of Golgi apparatus markers and LG-associated proteins together with transglutaminase 1, because LG are thought to be a part of continuous tubular network originated from Golgi apparatus to the cell membrane. In this point of view, we employed antibodies to well-established marker molecules of each part of Golgi apparatus-LG-cell membrane network, i.e. GM130 antibody, anti-TGN-46 antibody and anti-transglutaminase 1 antibody (B.C1) as markers for *cis*-Golgi, *trans*-Golgi and cell membrane, respectively. Our results showed that ABCA12 localized throughout the entire Golgi apparatus to LG at the cell periphery mainly in the granular layer keratinocytes. These results suggest that ABCA12 works in lipid transport from Golgi apparatus to LG in the granular layer cells.

Materials and methods

Antibodies

Polyclonal anti-ABCA12 antiserum was raised in rabbit (21). The other primary antibodies used in the present study were mouse monoclonal anti-glucosylceramide antibody (Alexis Biochemicals, San Diego, CA, USA) for immunofluorescent labelling, rabbit polyclonal anti-glucosylceramide antibody (Glycobiotech, Kuekel, Germany) for immunoelectron microscopic labelling, sheep polyclonal anti-TGN-46 antibody (Serotec Inc., Oxford, UK), anti-transglutaminase 1 antibody, B.C1 (Biomedical Technologies Inc., Stoughton, MA, USA) and GM130 (BD Biosciences, San Jose, CA, USA).

Cell culture

Normal human keratinocytes were purchased from Lonza Walkersville Inc., (Walkersville, MD, USA) and were grown in defined keratinocyte serum-free medium (SFM) (Invitrogen, San Diego, CA, USA). All the cells were maintained at 37°C in a 5% CO_2 atmosphere.

In order to induce keratinization, both cells were cultured with high-concentration calcium medium (Ca^{2+} = 1.2 mM) for 48 h.

Immunofluorescent labelling

Immunofluorescent labelling was performed as previously described (29). Briefly, 5-μm-thick sections of patients' fresh unfixed skin samples and control normal skin samples cut using a cryostat or keratinocytes cultured in the chamber slides were prepared for immunolabelling. The sections and cells were incubated in primary antibody solution for 30 min at 37°C. Antibody dilutions were as follows: 1/10 for anti-glucosylceramide antibody, 1/4 for anti-TGN-46 antibody, 1/10 for anti-transglutaminase 1 antibody B.C1 and 1/10 for GM130.

The sections were then incubated in fluorescein isothiocyanate (FITC)-conjugated to rabbit anti-mouse immunoglobulins or goat anti-rabbit immunoglobulins diluted 1 : 50 (Jackson ImmunoResearch, Baltimore Pike, USA) for 30 min at 37°C, followed by 10 μg/ml of propidium iodide (Sigma Chemical Co., St. Louis, MO, USA) nuclear counterstain for 10 min. For double labelling, FITC-conjugated and tetramethylrhodamine-isothiocyanate (TRITC)-conjugated secondary antibodies were used to label deposits of rabbit polyclonal anti-*ABCA12* antiserum and mouse monoclonal antibodies, respectively. Nuclear staining was performed using TO-PRO-3 (Invitrogen, Carlsbad, CA, USA) in the double-labelled sections. The sections were extensively washed with phosphate-buffered saline (PBS) between incubations. The stained sections were then mounted with a cover slip in 50% glycerol-based mounting medium and observed by a confocal laser scanning microscope.

Postembedding immunogold electron microscopy using cryofixed, cryosubstituted samples

Normal human skin samples were obtained from surgical operations of the benign subcutaneous skin tumors under fully informed consent, and were processed for postembedding immunoelectron microscopy as previously described (30). Cyrofixed, cryosubstituted samples were embedded in Lowicryl K11M resin. Ultrathin sections were cut and incubated with rabbit polyclonal anti-*ABCA12* antisera or rabbit polyclonal anti-glucosylceramide antibody, a secondary linker antibody and a 5-nm gold-conjugated antibody for immunogold labelling.

Ultrathin cryosections (0.1–0.2-μm thick)

Ultrathin cryosections of normal human skin were obtained basically according to a method described by Tokuyasu in 1980 (31), with some modifications (32). Fresh normal human skin obtained at surgery was cut into

small pieces (<1 mm^3), prefixed with 2% paraformaldehyde at room temperature for 2 h, and with 100 mM glycine in Dulbecco's PBS at room temperature for. 2 h and with 2.3 M sucrose in phosphate buffer at 4°C for 2 days. The samples were mounted on pins, rapidly frozen by liquid propane plunging (at −196°C), and stored in liquid nitrogen until required. Semi-thin sections were cut from the surface of the samples at −80 to −100°C using an Ultracut-S ultramicrotome equipped with a FCS cryosystem (Reichert-Jung, Vienna, Austria). Then, ultrathin sections (0.2-μm thick) were cut, transferred to albumin-coated glass slides using a platinum loop containing a droplet of 2.3 M sucrose/PBS, and processed as substrate for immunofluorescence labelling. For immunogold electron microscopy, ultrathin sections (0.1-μm thick) were also cut from a block, transferred to Formvar-coated nickel grids and processed for immunolabelling.

Results

Immunofluorescent double labelling revealed *ABCA12* and glucosylceramide co-localized within the granular layer keratinocytes

In normal human epidermis, ABCA12 is expressed in the entire epidermis, mainly in the upper spinous and granular layers (Fig. 1b,e,h,k). With non-specific background staining in the basal layer cells, the ABCA12 immunoreactivity seemed to be stronger than the true expression level. Glucosylceramide, a major lipid component of LG (33–35) was seen in the granular layer in the epidermis (Fig. 1a). TGase1, a membrane-bound enzyme essential for cornified cell envelope formation, was expressed at the cell periphery of the upper spinous and granular layer cells (Fig. 1d). TGN46, a trans-Golgi marker, was seen in the cytoplasm of all the epidermal cells (Fig. 1g). Perinuclear small dots staining of GM130, a *cis*-Golgi marker, was seen in the cytoplasm of keratinocytes in all epidermal layers (Fig. 1j). Immunofluorescent double labelling revealed that the majority of ABCA12 co-localized with glucosylceramide in the cytoplasm within the upper spinous and granular cells (Fig. 1c). ABCA12 seemed to partly co-localize with TGase1 (Fig. 1f). ABCA12 and TGN46 showed no apparent overlapping staining in the epidermis *in vivo* and only TGN46 expression was seen in the spinous layer cells (Fig. 1i). GM130 immunolabelling was seen mainly in the lower epidermis and no apparent co-localization of GM130 and ABCA12 was observed *in vivo* (Fig. 1l).

In cultured keratinocytes, ABCA12 is distributed from Golgi apparatus to the cell periphery

In normal human keratinocytes cultured under high Ca^{2+} conditions, the majority of ABCA12 and glucosylceramide co-localized in the cytoplasm (Fig. 2a–c). ABCA12 and

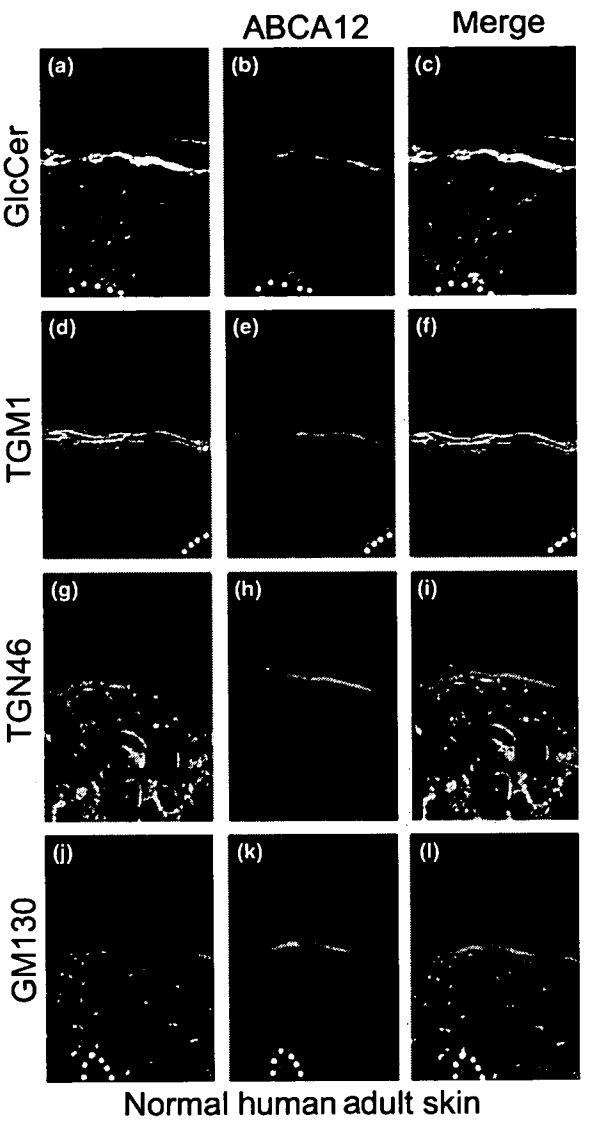

Figure 1. Double immunolabelling for ABCA12 and other molecules using conventional cryostat sections of normal human skin. (a–c) Double immunolabelling with anti-glucosylceramide (GlcCer) antibody and anti-ABCA12 antibody. GlcCer and ABCA12 immunolabelling overlapped in the cytoplasm of granular layer keratinocytes (c). (d–f) Double immunolabelling with anti-TGase1 antibody and anti-ABCA12 antibody. Both TGase1 and ABCA12 immunostaining were observed mainly in the granular layer cells and they partly overlapped (f). (g–i) Double immunolabelling with anti-TGN46 antibody and anti-ABCA12 antibody. TGN46 was detected in the cytoplasm of the spinous and granular layer cells (g,h). TGN46 and ABCA12 immunostaining showed no apparent overlap (i). (j–l) Double immunolabelling with anti-GM130 antibody and anti-ABCA12 antibody. Small, punctuate cytoplasmic staining was observed in the spinous and granular layer cells with anti-GM130 antibody (j). GM130 immunostaining did not overlap apparently with anti-ABCA12 antibody staining in the epidermis (l). ABCA12, red (TRITC); GlcCer, TGase1, TGN46, GM130, green (fluorescein isothiocyanate); nuclear stain, blue (TO-PRO-3). White dots, dermoepidermal junction. Magnification ×40.

TGase1 failed to co-localize. TGase1 staining showed a peripheral plasma membrane-associated pattern at the cell periphery (Fig. 2d–f). *ABCA12* staining was proximal to the TGase1 staining.

ABCA12 and TGN46 co-localized in part in the cytoplasm (Fig. 2g–i). GM130 staining was seen in the perinuclear area whereas the majority of GM130 was co-localized with ABCA12 around the perinuclear cytoplasm, although only ABCA12 staining extended to the cell periphery (Fig. 2j–l).

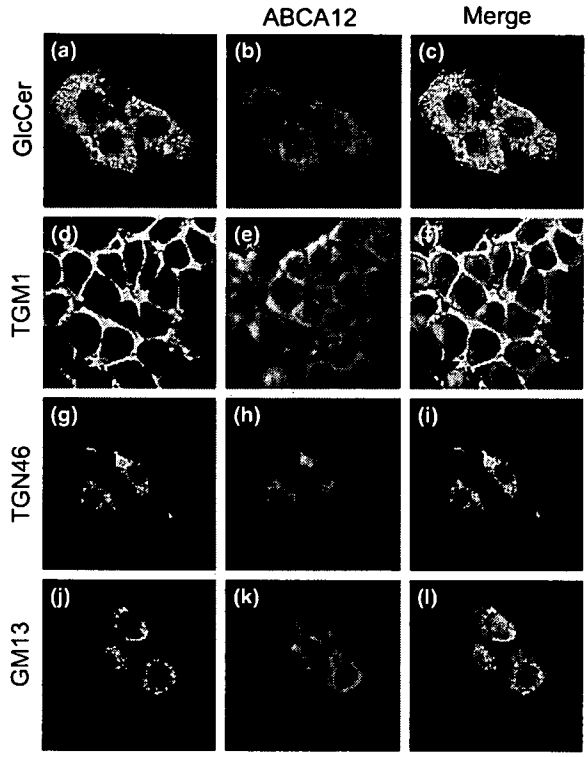

Figure 2. Double immunolabelling for ABCA12 and other molecules in normal cultured human epidermal keratinocytes. (a–c) Double immunolabelling with anti-glucosylceramide (GlcCer) antibody and anti-ABCA12 antibody. Both GlcCer immunostaining and ABCA12 immunolabelling were diffusely observed in the cultured keratinocyte cytoplasm (a,b). GlcCer and ABCA12 immunolabelling almost completely overlapped in the cytoplasm (c). (d–f) Double immunolabelling with anti-TGase1 antibody and anti-ABCA12 antibody. TGase1 seemed to be restricted to the cell membrane (d) and ABCA12 was observed diffusely within the cytoplasm (e) of the cultured keratinocytes. The immunostaining rarely overlapped (f). (g–i) Double immunolabelling with anti-TGN46 antibody and anti-*ABCA12* antibody. TGN46 was detected in the cultured keratinocyte cytoplasm (g). ABCA12 was rather diffusely distributed in the cytoplasm (h). Most TGN46 co-localized with ABCA12 (yellow colour) (i). (j–l) Double immunolabelling with anti-GM130 antibody and anti-ABCA12 antibody. GM130 was detected in the cultured keratinocyte cytoplasm, mainly in the perinuclear area (j). Most of GM130 co-localized with ABCA12 (yellow colour) in the perinuclear area, but at the cell periphery only ABCA12 immunostaining was observed without GM130 labelling (l). ABCA12, red (TRITC); GlcCer, TGase1, TGN46, GM130, green (fluorescein isothiocyanate); nuclear stain, blue (TO-PRO-3). Magnification ×60.

Postembedding immunoelectron microscopic observation revealed that both *ABCA12* and glucosylceramide localized to LG

Postembedding immunoelectron microscopy revealed that both ABCA12 and glucosylceramide were observed in the LG of the uppermost granular layer keratinocytes (Fig. 3). In the granular layer cells, there was no apparently labelled

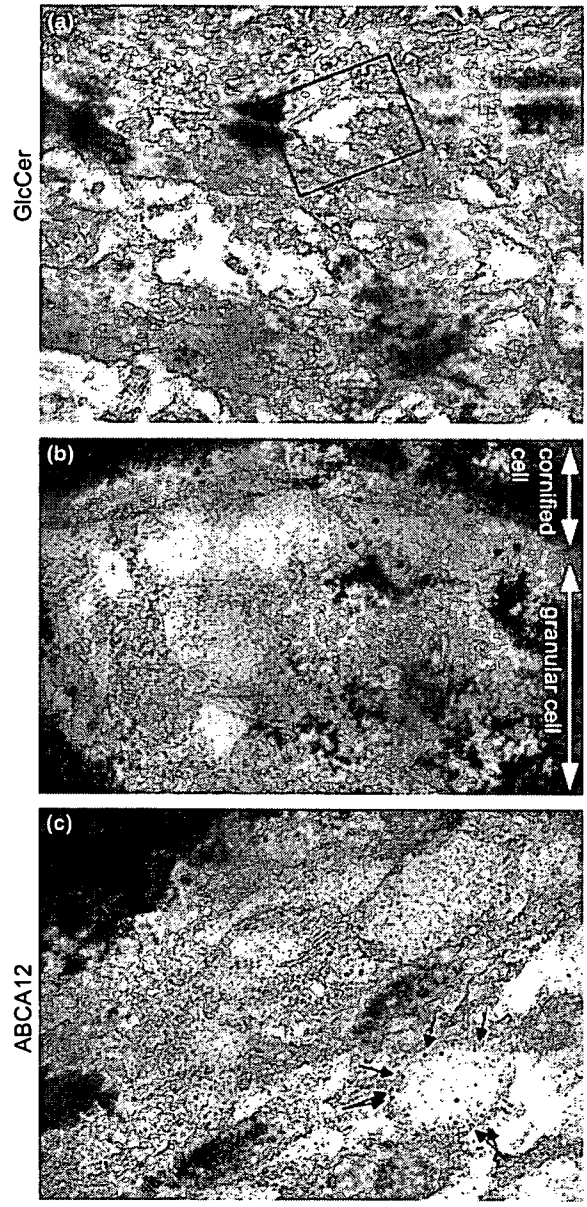

Figure 3. Cryosubstitution, cryofixation postembedding immunoelectron microscopy with anti-ABCA12 antibody and anti-glucosylceramide antibody. The apical border of the granular layer cell was observed (a). 5-nm gold labellings for glucosylceramide (b) and ABCA12 (c) were observed in the lamellar granules (LG) in the cytoplasm of the granular layer cells. ABCA12 labelling were seen on the LG (c, arrows). Magnification ×20 000 (a), ×1 00 000 (b), ×50 000 (c).

structure other than LG. Glucosylceramide was secreted from the LG to the intercellular space in the stratum corneum.

Cryoultramicrotomy

Ultrathin cryosections demonstrated highly preserved, easy to visualize plasma membrane ultrastructure of LG and intercellular lipid layers. In addition, immunofluorescence labelling on ultrathin cryosections clearly revealed a localization of ABCA12 and glucosylceramide. Using immunofluorescence labelling at the light microscopic level, ABCA12 and glucosylceramide staining almost completely overlapped within the granular layer keratinocytes (Fig. 4). By immunoelectron microscopy using ultrathin cryosections, glucosylceramide labelling was seen with the lamellar structures in the LG (Fig. 5a,b). ABCA12 immunogold labelling was observed on or close to the membrane surrounding LG in the uppermost granular layer cells (Fig. 5c,d).

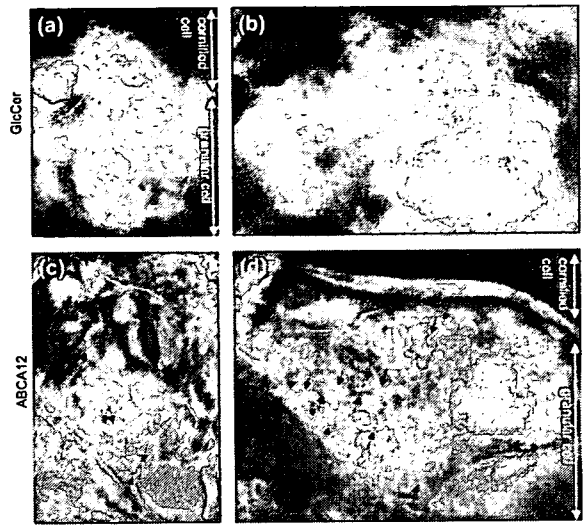

Figure 5. Cryoultramicrotomy for ABCA12 and glucosylceramide. Immunogold electron microscopic observation on ultrathin cryosections of normal human skin showed an apparent glucosylceramide (5-nm gold particles) labelling of the lamellar structure inside the lamellar granules (LG) (a,b). ABCA12 (5-nm gold particles) localized to LG containing lamellar structures (c,d). Magnification ×50 000 (a,b), ×30 000 (c,d).

Discussion

ABCA12 belongs to a large superfamily of ABC transporters, which bind ATP in the transport of various molecules across membranes (2–4). The ABCA subfamily is thought to act as lipid transporters (5).

ABCA3 was thought to work in lipid transport in type II alveolar cells in alveolar surfactant formation (36) and loss of function mutations in ABCA3 lead to fatal surfactant deficiency in the neonate (37). Finally, defects in *ABCA12* were identified as the cause of HI and lamellar ichthyosis (21,22,38).

ABCA2, *ABCA3* and *ABCA7* mRNA levels were reported to be upregulated after sustained cholesterol influx (39,40), suggesting that ABCA transporters are involved in transmembrane transport of endogenous lipids (15). From these facts, transporters in the ABCA subfamily were thought to be involved in transmembrane transport of endogenous lipids (14,16,17).

In the present study, we have demonstrated that the majority of ABCA12 was distributed in the granular layer cells associated with glucosylceramide. Double-labelling immunofluorescence staining in cultured keratinocytes clearly indicated that ABCA12 was localized from Golgi apparatus (co-localized with *cis*-Golgi marker GM130 and *trans*-Golgi marker TGN-46) to cell periphery (close to the plasma membrane stained with transglutaminase 1). In the epidermis *in vivo*, GM130 was expressed equally from the basal cells to the granular layer cells, although *ABCA12* was expressed mainly in the granular layer cells. Thus, co-localization of ABCA12 and GM130 was seen only in the limited area in the granular layers of the epidermis *in vivo*. ABCA12 failed to co-localize with TGase1, a cell membrane-bounding protein, both *in vivo* and in the cultured keratinocytes, and ABCA12 was thought to be distributed only very sparsely, on the cell membrane.

Furthermore, postembedding immunoelectron microscopy and cryoultramicrotomy revealed that ABCA12 was located on LG in the uppermost granular layer cells. Glucosylceramide was seen on the lamellar structures inside

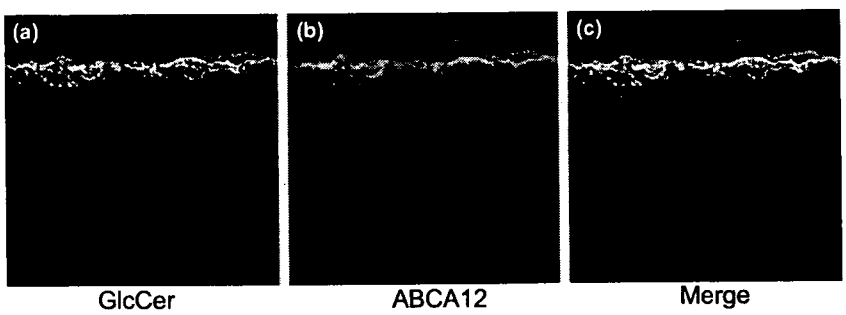

Figure 4. Immunofluorescence labelling using ultrathin cryosections for ABCA12 and glucosylceramide. Immunofluorescence labelling on ultrathin cryosections clearly demonstrated that glucosylceramide (a) and ABCA12 (b) overlapped in the cytoplasm of the granular layer cells (c). ABCA12, red (TRITC); GlcCer, green (fluorescein isothiocyanate); nuclear stain, blue (TO-PRO-3). Magnification ×100.

the LG and was subsequently secreted to the intercellular space. Taking all these findings into consideration, in the uppermost granular layer cells, ABCA12 was thought to be distributed to the Golgi apparatus limiting membrane and subsequently to LG containing glucosylceramide at the keratinocyte periphery. These results supported our hypothesis that *ABCA12* is working in lipid transport from the Golgi apparatus to LG in the uppermost granular layer cells (Fig. 6).

LG are known as lipid-transporting granules and LG contents are secreted to the intercellular space forming intercellular lipid layers between the stratum corneum corneocytes, which is essential for the skin barrier function. Recently, it was shown that LG are not true granules, but are tubular structures distended from the *trans*-Golgi network (34,41,42). LG may have their own unique trafficking and secretory systems. Considering our results that ABCA12 was localized from the Golgi apparatus to LG at the cell periphery, this supports the hypothesis that ABCA12 is likely to be a membrane lipid transporter that functions in the lipid transport from the *trans*-Golgi network to LG at the keratinocyte periphery. In this context, the LG abnormality in HI resulting from loss of ABCA12 function probably causes a blockade of the normal lipid transport and secretion and leads to congestion of the lipid flow within the keratinocyte.

Acknowledgements

The authors thank Ms Megumi Sato and Ms Maki Goto for their fine technical assistance on this project. This work was supported in part by grant-in-aid from the Ministry of Education, Science, Sports, and Culture of Japan to M. Akiyama (Kiban B 18390310) and to H. Shimzu (Kiban A 17209038).

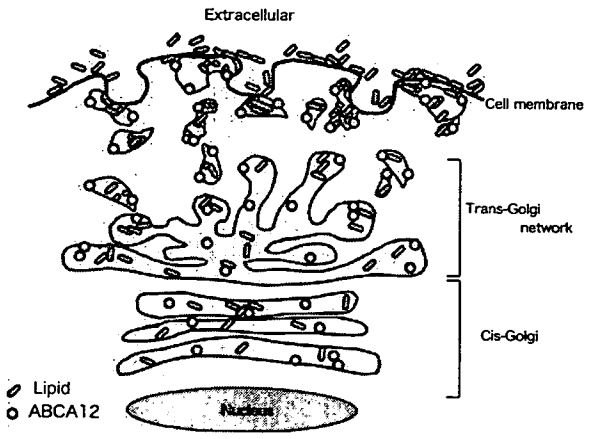

Figure 6. Hypothetical scheme of ABCA12 distribution at the apical border of differentiated epidermal keratinocytes. The lipid transporter ABCA12 was localized to the membrane from the Golgi apparatus to the lamellar granules (LG). ABCA12 is thought to be associated with lipid transport from the Golgi apparatus to cell periphery where these lipids are secreted from LG in the uppermost granular layer cells.

References

1 Higgins C F. ABC transporters: from microorganisms to man. Annu Rev Cell Biol 1992: **8**: 67–113.
2 Allikmets R, Gerrard B, Hutchinson A, *et al.* Characterization of the human ABC superfamily: isolation and mapping of 21 new genes using the expressed sequence tags database. Hum Mol Genet 1996: **5**: 1649–1655.
3 Dean M, Rzhetsky A, Allikmets R, *et al.* The human ATP-binding cassette (ABC) transporter superfamily. Genome Res 2001: **11**: 1156–1166.
4 Borst P, Elferink R O. Mammalian ABC transporters in health and disease. A Rev Biochem 2002: **71**: 537–592.
5 Peelman F, Labeur C, Vanloo B, *et al.* Characterization of the ABCA transporter subfamily: identification of prokaryotic and eukaryotic members, phylogeny and topology. J Mol Biol 2003: **325**: 259–274.
6 Klein I, Sarkadi B, Varadi A. An inventory of the human ABC proteins. Biochim Biophys Acta 1999: **1461**: 237–262.
7 Akiyama M. Pathomechanisms of Harlequin ichthyosis and ABCA transporters in human diseases. Arch Dermatol 2006: **142**: 914–918.
8 Akiyama M. Harlequin ichthyosis and other autosomal recessive congenital ichthyoses: the underlying genetic defects and pathomechanisms. J Dermatol Sci 2006: **42**: 83–89.
9 Brooks-Wilson A, Marcil M, Clee S M, *et al.* Mutations in ABC1 in Tangier disease and familial high-density lipoprotein deficiency. Nat Genet 1999: **22**: 336–345.
10 Rust S, Rosier M, Funke H, *et al.* Tangier disease is caused by mutations in the gene encoding ATP-binding cassette transporter 1. Nat Genet 1999: **22**: 352–355.
11 Oram J F. Molecular basis of cholesterol homeostasis: lessons from Tangier disease and ABCA1. Trends Mol Med 2002: **8**: 168–173.
12 Allikmets R, Shroyer N F, Singh N *et al.* Mutation of the Stargardt disease gene (ABCR) in age-related macular degeneration. Science 1997: **277**: 1805–1807.
13 Allikmets R. Simple and complex ABCR: genetic predisposition to retinal disease. Am J Hum Genet 2000: **67**: 793–799.
14 Hayden M R, Clee S M, Brooks-Wilson A, *et al.* Cholesterol efflux regulatory protein, Tangier disease and familial high-density lipoprotein deficiency. Curr Opin Lipidol 2000: **11**: 117–122.
15 Schmitz G, Langmann T. Structure, function and regulation of the ABC1 gene product. Curr Opin Lipidol 2001: **12**: 129–140.
16 Orso E, Broccardo C, Kaminski W E, *et al.* Transport of lipids from Golgi to plasma membrane is defective in Tangier disease patients and Abc1-deficient mice. Nat Genet 2000: **24**: 192–196.
17 Weng J, Mata N L, Azarian S M, *et al.* Insights into the function of Rim protein in photoreceptors and etiology of Stargardt's disease from the phenotype in abcr knockout mice. Cell 1999: **98**: 13–23.
18 Kielar D, Kaminski W E, Liebisch G, *et al.* Adenosine triphosphate binding cassette (ABC) transporters are expressed and regulated during terminal keratinocyte differentiation: a potential role for ABCA7 in epidermal lipid reorganization. J Invest Dermatol 2003: **121**: 465–474.
19 Jiang Y J, Lu B, Kim P, Elias P M, Feingold K R. Regulation of ABCA1 expression in human keratinocytes and murine epidermis. J Lipid Res 2006: **47**: 2248–2258.
20 Lee H K, Nam G W, Kim S H, Lee S H. Phytocomponents of triterpenoids, oleanolic acid and ursolic acid, regulated differently the

processing of epidermal keratinocytes via PPAR-alpha pathway. Exp Dermatol 2006: **15**: 66–73.

21 Akiyama M, Sugiyama-Nakagiri Y, Sakai K, *et al.* Mutations in ABCA12 in Harlequin ichthyosis and functional rescue by corrective gene transfer. J Clin Invest 2005: **115**: 1777–1784.

22 Kelsell D P, Norgett E E, Unsworth H, *et al.* Mutations in ABCA12 underlie the severe congenital skin disease Harlequin ichthyosis. Am J Hum Genet 2005: **76**: 794–803.

23 Akiyama M, Sakai K, Sugiyama-Nakagiri Y, *et al.* Compound heterozygous mutations including a *de novo* missense mutation in ABCA12 led to a case of Harlequin ichthyosis with moderate clinical severity. J Invest Dermatol 2006: **126**: 1518–1523.

24 Rajpar S F, Cullup T, Kelsell D P, Moss C. A novel ABCA12 mutation underlying a case of Harlequin ichthyosis. Br J Dermatol 2006: **155**: 204–206.

25 Akiyama M, Sakai K, Wolff G, *et al.* A novel ABCA12 mutation 3270delT causes Harlequin ichthyosis. Br J Dermatol 2006: **155**: 1064–1066.

26 Thomas A C, Cullup T, Norgett E E, *et al.* ABCA12 is the major Harlequin ichthyosis gene. J Invest Dermatol 2006: **126**: 2408–2413.

27 Akiyama M, Titeux M, Sakai K, *et al.* DNA-based prenatal diagnosis of Harlequin ichthyosis and characterization of ABCA12 mutation consequences. J Invest Dermatol 2007: **127**: 568–573.

28 Akiyama M, Sakai K, Sato T, *et al.* Compound heterozygous *ABCA12* mutations including a novel nonsense mutation underlie Harlequin ichthyosis. Dermatology (in press).

29 Akiyama M, Smith L T, Yoneda K, *et al.* Periderm cells form cornified cell envelope in their regression process during human epidermal development. J Invest Dermatol 1999: **112**: 903–909.

30 Shimizu H, McDonald J N, Kennedy A R, *et al.* Demonstration of intra- and extra-cellular localization of bullous pemphigoid antigen using cryofixation and freeze substitution for postembedding immuno-electron microscopy. Arch Dermatol Res 1989: **281**: 443–448.

31 Tokuyasu K T. Immunochemistry on ultrathin frozen sections. Histochem J 1980: **12**: 381–403.

32 Ishiko A, Shimizu H, Masunaga T, Kurihara Y, Nishikawa T. Detection of antigens by immunofluorescence on ultrathin cryosections of skin. J Histochem Cytochem 1998: **46**: 1455–1460.

33 Vielhaber G, Pfeiffer S, Brade L, *et al.* Localization of ceramide and glucosylceramide in human epidermis by immunogold electron microscopy. J Invest Dermatol 2001: **117**: 1126–1136.

34 Ishida-Yamamoto A, Simon M, Kishibe M, *et al.* Epidermal lamellar granules transport different cargoes as distinct aggregates. J Invest Dermatol 2004: **122**: 1137–1144.

35 Holleran W M, Takagi Y, Menon G K, *et al.* Processing of epidermal glucosylceramides is required for optimal mammalian cutaneous permeability barrier function. J Clin Invest 1993: **91**: 1656–1664.

36 Yamano G, Funahashi H, Kawanami O, *et al.* ABCA3 is a lamellar body membrane protein in human lung alveolar type II cells. FEBS Lett 2001: **508**: 221–225.

37 Shulenin S, Nogee L M, Annilo T, Wert S E, Whitsett J A, Dean M. ABCA3 gene mutations in newborns with fatal surfactant deficiency. N Engl J Med 2004: **350**: 1296–1303.

38 Lefèvre C, Audebert S, Jobard F, *et al.* Mutations in the transporter ABCA12 are associated with lamellar ichthyosis type 2. Hum Mol Genet 2003: **12**: 2369–2378.

39 Kaminski W E, Piehler A, Pullmann K, *et al.* Complete coding sequence, promoter region, and genomic structure of the human ABCA2 gene and evidence for sterol-dependent regulation in macrophages. Biochem Biophys Res Commun 2001: **281**: 249–258.

40 Klucken J, Buchler C, Orso E, *et al.* ABCG1 (ABC8), the human homolog of the *Drosophila* white gene, is a regulator of macrophage cholesterol and phospholipid transport. Proc Natl Acad Sci USA 2000: **97**: 817–822.

41 Norlen L. Skin barrier formation: the membrane folding model. J Invest Dermatol 2001: **117**: 823–829.

42 Norlen L, Al-Amoudi A, Dubochet J. A cryotransmission electron microscopy study of skin barrier formation. J Invest Dermatol 2003: **120**: 555–560.

FEBS Letters 581 (2007) 535–540

Gelsolin segment 5 inhibits HIV-induced T-cell apoptosis via Vpr-binding to VDAC

Hongjiang Qiao*, James R. McMillan

Department of Dermatology, Hokkaido University Graduate School of Medicine, Kita-15, Nishi-7, Kita-Ku, Sapporo 060-0815, Japan
Creative Research Initiative, Faculty of Science, Hokkaido University, Kita-15, Nishi-7, Kita-Ku, Sapporo 060-0815, Japan

Received 25 October 2006; revised 19 December 2006; accepted 28 December 2006

Available online 17 January 2007

Edited by Richard Marais

Abstract **Viral protein R (Vpr) from the human immunodeficiency virus induces cell cycle arrest in proliferating cells, stimulates virus transcription, and regulates activation and apoptosis of infected T-lymphocytes. We report that Jurkat cells overexpressing full-length gelsolin show resistance to Vpr-induced T-cell apoptosis with abrogation of mitochondrial membrane potential loss and the release of cytochrome *c*. Co-immunoprecipitation assays in HEK293T cells demonstrated that overexpression of full-length or segment 5 (G5) but not G5-deleted gelsolin (ΔG5) bound to the voltage-dependent anion channel (VDAC), and that the G5 subunit can inhibit HIV-1-Vpr-binding to VDAC. We also confirmed that full-length gelsolin has the same effect in Jurkat cells. Clonogenic analysis showed that transfection of G5 but not ΔG5 cDNA protects Jurkat T cells from HIV-Vpr-Tet induced T-cell apoptosis and promoted cell survival, as did full-length gelsolin. These results suggest that the gelsolin G5 domain inhibits HIV-Vpr-induced T-cell apoptosis by blocking the interaction between Vpr and VDAC, and might be used as a protective treatment against HIV-Vpr-induced T-cell apoptosis.**

Keywords: Cytoskeletal protein; AIDS; Mitochondria; Cell death

1. Introduction

Multiple mechanisms have been proposed to explain the death and dysfunction of CD4+ T-cells after infection with the human immunodeficiency virus type 1 (HIV-1) [1]. There are various molecular HIV-1 components that play a role in the induction of apoptosis in T-lymphocytes [1]. Viral protein R (Vpr) plays an important role in regulating the nuclear transport of the HIV-1 pre-integration complex, and is required for virus replication in non-dividing cells [2,3]. Vpr also induces cell cycle arrest in proliferating cells, stimulates virus transcription, and regulates activation and apoptosis in infected cells [2,4,5]. These changes occur in the absence of other viral gene products, suggesting that Vpr mediates its proviral effects at least partially or perhaps solely, through modulation of the state of the target cell rather than directly by the virus [3]. Vpr from HIV-1 attaches to mitochondrial membranes and induces mitochondrial membrane permeabilization (MMP), which is a critical step in the regulation of apoptosis and is often accompanied by mitochondrial swelling and fragmentation [6,7].

Gelsolin, an actin-regulatory protein that modulates actin assembly and disassembly, is found as both an intrinsic cytoplasmic protein and secreted plasma protein [8,9]. In addition, gelsolin was identified as a substrate for caspase-3 by screening the translation products of small complementary DNA pools for sensitivity to cleavage by caspase-3 [10]. Expression of gelsolin cleavage product in multiple cell types caused the cells to detach, round up, and undergo nuclear fragmentation [10]. It was proposed that its association with actin drives the calcium-independent activation of the N-terminal three domains gelsolin G1–G3 during apoptosis [11]. Conversely, some reports have previously shown that cytoplasmic gelsolin is also present in the mitochondrial fraction of cells, and that full-length gelsolin can inhibit apoptosis of human Jurkat T-cells [12,13]. The overexpression of gelsolin inhibits the loss of mitochondrial membrane potential and cytochrome *c* release from mitochondria, resulting in a lack of activation of caspase −3, −8, and −9 in Jurkat cells treated with staurosporine, thapsigargin, and protoporphyrin IX [13]. This anti-apoptotic function of gelsolin was also observed in butyrate-induced apoptosis of colorectal cancer cells and the cholinergic toxin ethylcholine aziridinium-or amyloid-beta-induced apoptosis of neuronal cells [14–17], and segment G5 of human cytoplasmic gelsolin is sufficient for the function recorded in the latter case [17].

In this study, our efforts were directed towards investigating whether gelsolin can inhibit HIV-Vpr-induced cell death in Jurkat T cells, and to determine the specific gelsolin domain responsible for that function.

2. Results

2.1. Resistance of gelsolin-overexpressed Jurkat T-cells to HIV-Vpr-induced apoptosis

In an effort to determine whether overexpression of gelsolin in Jurkat T-cells affects HIV-Vpr-induced apoptosis, we used human cytoplasmic gelsolin-stably overexpressed in a Jurkat

*Corresponding author. Fax: +81 11 706 7869.
E-mail address: qiao@igm.hokudai.ac.jp (H. Qiao).

Abbreviations: HIV-1, human immunodeficiency virus type 1; Vpr, viral protein R; VDAC, voltage-dependent anion channel; MMP, mitochondrial membrane permeabilization; IB, immunoblotting; Dox, doxycycline; PTPC, permeability transition pore complex; ANT, adenine nucleotide translocator; NMDA, *N*-methyl-D-aspartate; VDCC, voltage-dependent calcium channels; rtTA, reverse tetracycline-controlled transactivator; PI, propidium iodide; IP, immunoprecipitation

0014-5793/$32.00
doi:10.1016/j.febslet.2006.12.057

T-cell clone JGF that was previously established [12]. To confirm continuous expression of gelsolin in JGF and Neo control clone JNF cells, immunoblotting (IB) analysis was performed. Gelsolin was not detected in JNF, while JGF displayed expression of gelsolin (90 KD) and was in keeping with previous results (Fig. 1A). The level of actin remained unchanged among all cell lines. Since we were not able to acquire HIV-Vpr stable transfectants using a constitutively expressing Vpr plasmid, we used an inducible expression system based on the tetracycline-responsive operon (Tet-on system) [18]. Jurkat Tet-on cell lines were created as described in Section 4 below that stably express FLAG-tagged HIV-Vpr by selection in medium containing hygromycin and zeocin. Several clones derived from cells transfected with HIV-Vpr were isolated, analyzed by IB analysis using anti-FLAG antibody to confirm the high expression of HIV-Vpr, and HIV-Vpr-overexpressed parental clone (JPV 5), JNF clones (JNFV 3, 4, 7) , and JGF clones (JGFV 2, 8, 9) were established. JP cells and all clone cells did not express HIV-Vpr under basic conditions (Fig. 1B). However, treatment with doxycycline (Dox) for 48 h resulted in a marked increase of recombinant Vpr protein expression without any detectable change in β-actin expression in parental cells and all clones. At different time points after Dox addition, JPV clone 5, JNFV clones (3, 4, 7) and JGF clones (2, 8, 9) were assayed for cell viability and apoptosis signs using Hoechst 33342 and PI staining. Hoechst 33342 staining showed HIV-Vpr-induced apoptosis accompanied by changes in nuclear morphology, such as nuclear condensation or fragmentation in control JNFV clones at 24, 48, 72 h after Dox treatment, while JGFV clones treated with Dox expressing HIV-Vpr failed to show any morphological nuclear changes (Fig. 2A). Cell viability analysis using Hoechst 33342 and PI revealed that all JGFV clones were clearly more resistant to apoptosis induced by Vpr compared to JPV clone 5 cells and all JNFV clones after 24 h (Dead cells: JGFV, 5% to JPV, 24%, JNFV, 23%), 48 h (Dead cells: JGFV, 9% to JPV, 46%, JNFV, 44%) and 72 h (Dead cells: JGFV, 12% to JPV, 55%, JNFV, 54%) (Fig. 2B) after initial Dox treatment. These data demonstrated that overexpression of gelsolin was associated with significant resistance to HIV-Vpr-induced apoptosis.

2.2. *Inhibition of mitochondrial membrane potential loss and cytochrome c release stimulated with HIV-Vpr in gelsolin-overexpressed Jurkat T cells*

Other report demonstrated that gelsolin can inhibit apoptosis induced by several apoptotic reagents by blocking signal transduction at the mitochondrial level upstream of the caspase cascade in human T lymphocytes [13]. To analyze the alteration in DeltaPsi(m) that follows HIV-Vpr apoptotic stimulation, we incubated cells after Dox treatment with the cationic dye Rhodamine 123 and then analyzed the cells using a flow-cytometer. JPV clone 5 and all JNF clones displayed loss of all mitochondrial potential, while JGFV clones demonstrated inhibitory activity (Fig. 3A). Another change observed in the mitochondria of apoptotic cells is the translocation of cytochrome *c* from within the innermost mitochondrial membrane to a cytosolic location. Immunoblot analysis of cytosolic fractions revealed that JPV clone 5 and all JNF clones showed cytochrome *c* release after Dox treatment, while there was almost no cytochrome *c* release from the JGF clones (Fig. 3B). Evaluation of all the data indicates that gelsolin

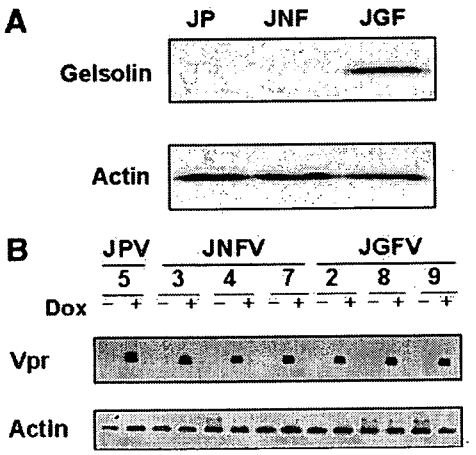

Fig. 1. Expression of gelsolin and HIV-Vpr in Jurkat cell lines by IB analysis. (A) Confirmation of stable expression of human full-length cytoplasmic gelsolin in Jurkat T cell line (JGF). JP, parental Jurkat cells; JNF, neo-transfected Jurkat clone. (B) Inducible expression of Flag-tagged HIV-Vpr in Jurkat Tet-on clones (JPV clone 5, JNFV clones 3, 4, 7, and JGFV clones 2, 8, 9) at 24 h in the absence or presence of 2 μg/ml Dox. The expression of actin was monitored to ensure equivalent loading and transfer.

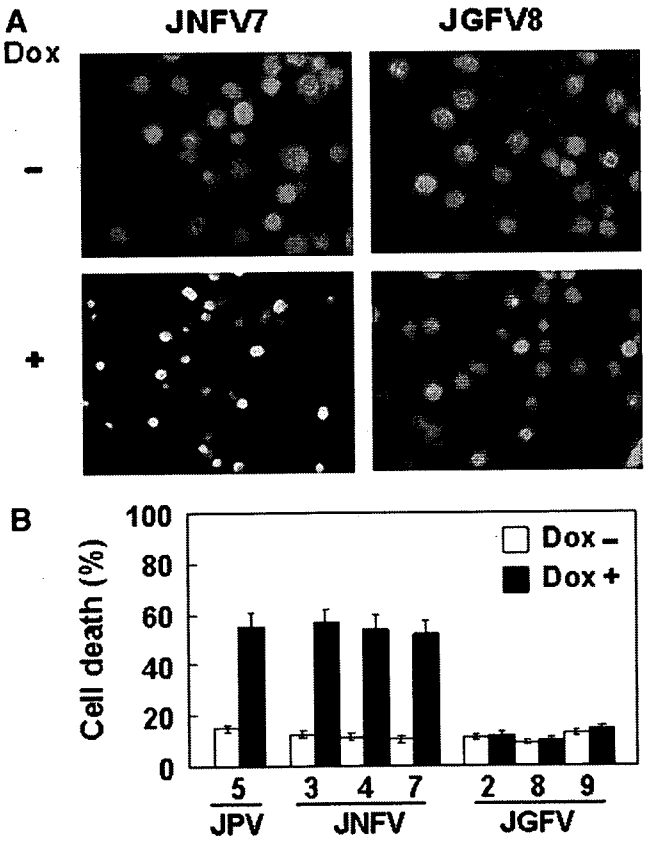

Fig. 2. Cell viability in HIV-Vpr expressed Jurkat cell lines. (A) Hoechst staining of HIV-Vpr expressed JNFV7 and JGFV8 cells at 72 h in the presence or absence of 2 μg/ml Dox. (B) Cell viability of JPV, JNFV, and JGFV cell lines at 72 h in the presence or absence of 2 μg/ml Dox was calculated as the percentage of apoptotic cells compared to total cells using Hoechst 33342 and PI. Three experiments were performed in duplicate, and values represent the mean + S.E. of dead cells.

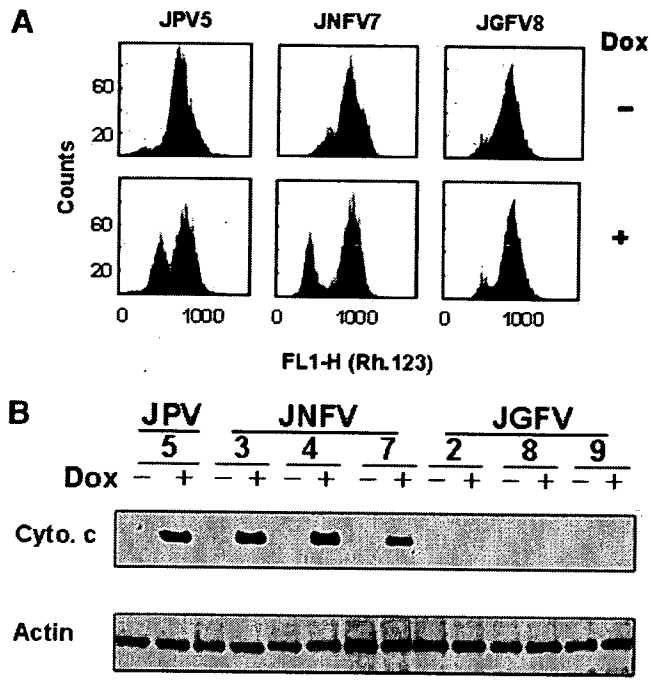

Fig. 3. MMP and cytochrome *c* release from mitochondria in HIV-Vpr expressed Jurkat cell lines. (A) MMP assessed by flow-cytometry with Rhodamine 123 of JPV5, JNFV7, and JGFV8 cells at 72 h in the presence or absence of 2 μg/ml Dox. (B) Cytochrome *c* release from mitochondria of JPV, JNFV, and JGFV cell lines at 72 h in the presence or absence of 2 μg/ml Dox.

can effectively inhibit HIV-Vpr-induced apoptosis at a point concomitant with, or upstream of, the mitochondrial events.

2.3. Inhibition of HIV-Vpr binding to VDAC by full-length gelsolin and gelsolin segment 5 (G5)

We have previously shown that segment 5 of gelsolin (G5) represents an important regulatory region in determining its inhibitory effect upon cell apoptosis [17]. Recent reports suggested that VDAC is a key molecule controlling apoptotic mitochondrial changes and the HIV-Vpr induces apoptosis via a direct effect on the mitochondrial permeability transition pore complex (PTPC) by binding VDAC [6]. To verify the interaction between full-length gelsolin, G5, and VDAC, co-immunoprecipitation experiments were performed. HEK293T cells were transiently transfected with an expression plasmid encoding Myc-tagged full-length gelsolin, G5, or G5-deleted gelsolin (ΔG5) together with expression plasmid encoding T7-tagged VDAC, and the cell lysates were immunoprecipitated with anti-Myc antibody. The resulting precipitates and a portion of the cell lysate were subjected to IB analysis with anti-T7 tag and anti-Myc antibodies. Results of IB analysis showed that VDAC coprecipitated with full-length gelsolin and the G5 domain, but not with ΔG5 transfectant, suggesting that gelsolin is physically associated with VDAC and that the G5 segment of gelsolin is necessary and by itself sufficient for this interaction (Fig. 4A).

The observed interaction allowed us to determine if gelsolin and HIV-Vpr compete for the binding of VDAC in cultured cells. HEK293T cells were transiently transfected with expression plasmids encoding Flag-tagged Vpr and T7-tagged VDAC, together with increasing amounts of expression plasmid for Myc-tagged G5 (Fig. 4B). Cell lysates were prepared from transfected cells, immunoprecipitated with anti-T7 tag antibody, and the resulting precipitates and a portion of cell lysate were subjected to IB analysis with anti-FLAG, anti-T7 tag and anti-Myc antibodies. The results of IB analysis showed that VDAC-bound-Vpr was reversibly reduced with the amount of G5 administered in a dose-dependent manner. The amounts of Vpr and VDAC expressed were almost constant. These results indicate that G5 blocks the interaction between HIV-Vpr and VDAC.

Therefore, we also examined the effect of full-length gelsolin on the physical interaction between Vpr and the VDAC in

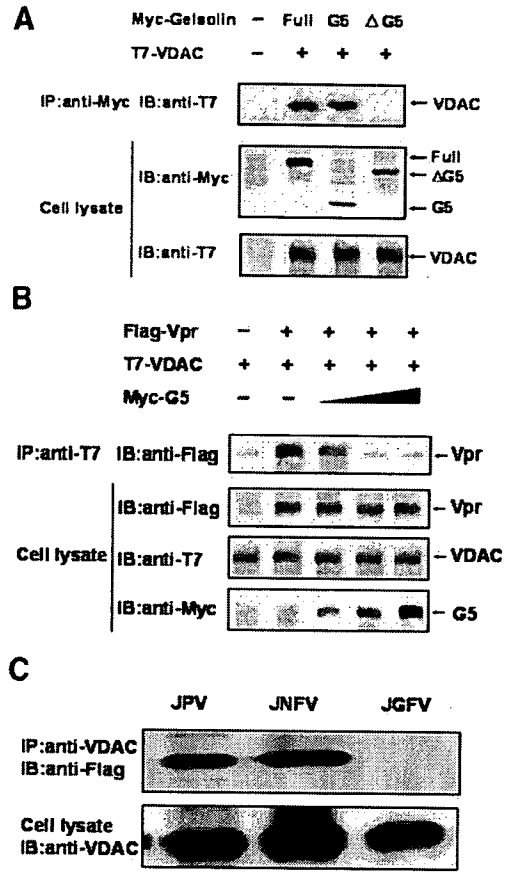

Fig. 4. Inhibition of VDAC-Vpr interaction by full-length gelsolin and the G5 segment of gelsolin. (A) HEK293T cells were transiently transfected with Myc-tagged full-length gelsolin (Full), G5 or ΔG5 (1 μg) together with T7-tagged VDAC (1 μg) as indicated. Cell lysates were subjected to immunoprecipitation (IP) with anti-Myc antibody, and the resulting precipitates were subjected to IB with anti-T7 tag antibody. A portion of the cell lysate was directly subjected to IB with anti-Myc, anti-T7 tag antibody in order to verify the expression level of gelsolin and VDAC proteins. (B) HEK293T cells were transfected with Flag-tagged HIV-Vpr and T7-tagged VDAC together with increasing amounts of Myc-G5 (0.5, 1, and 2 μg). Cell lysates were subjected to IP with anti-T7 tag antibody, and the resulting precipitates were subjected to IB with anti-FLAG antibody. A portion of the cell lysate was directly subjected to IB with anti-FLAG, anti-T7 tag, and anti-Myc antibodies to verify the expression level of Vpr, VDAC, and G5 proteins. (C) JPV, JNFV and JGFV cells were treated with Dox for 48 h. Cell lysates were subjected to IP with anti-VDAC antibody, and the resulting precipitates blotted with anti-Flag antibody. A portion of the cell lysate was directly subjected to IB with anti-VDAC in order to verify the VDAC protein expression level (internal control).

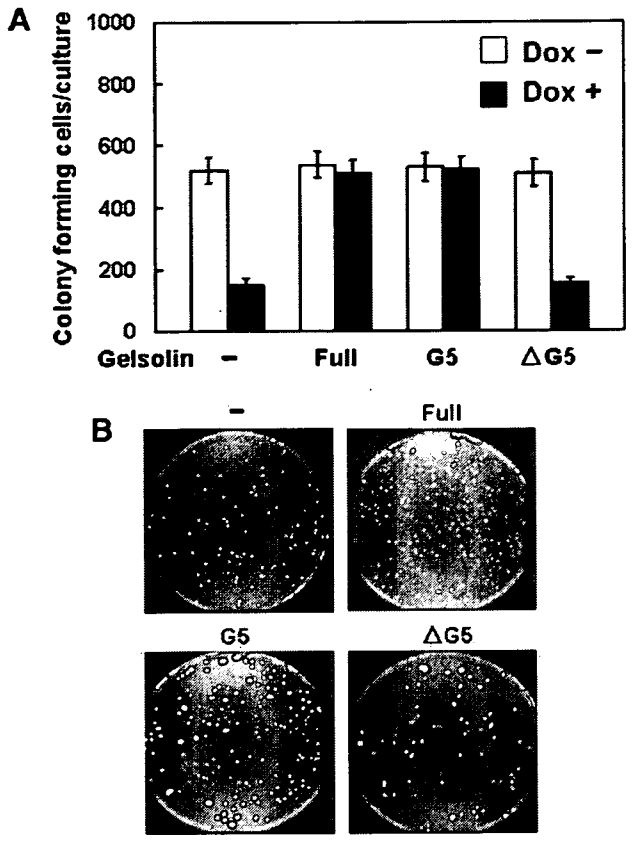

Fig. 5. G5 segment allows Dox-treated HIV-Vpr Tet-on Jurkat T cells to form colonies. (A) Cells were assayed for colony-forming ability 2 weeks after apoptotic induction by Dox treatment with the transfection of an empty plasmid (–), full-length gelsolin (Full), G5 or ΔG5 expression plasmids. Means and standard errors of two independent experiments each containing three replicates are shown. (B) Plates are illustrated below the corresponding Dox (+) columns of the histogram.

Jurkat cells, using an immunoprecipitation assay system (Fig. 4C). Cells were treated with Dox after 48 h, cell lysates were immunoprecipitated with anti-VDAC and the immunocomplexes probed with Flag tagged Vpr or gelsolin antibodies. These results showed that Vpr can interact with VDAC in JPV and JNFV cells, but this interaction cannot be detected in JGFV cells. These results demonstrate that Vpr is bound to VDAC in JPV clones and all JNFV clones, but this interaction was inhibited by full-length gelsolin overexpressing Jurkat cells after Dox treatment.

2.4. Protective function of G5 from HIV-Vpr-induced apoptosis in Jurkat T cells

In order to determine the protective function of full-length gelsolin and G5 from HIV-Vpr-induced apoptosis in the Jurkat cell line, we examined their effects by utilizing the most stringent criterion for cell survival: the ability to form a colony from only a single cell. Treatment of Dox in parental Jurkat HIV-Vpr Tet-on (JPV) clone 5 cell line with an empty control plasmid produced a substantial reduction in colonies that subsequently formed in soft agar (Fig. 5A and B). The transfection of expression plasmids with full-length gelsolin or G5, however, produced a 3.4-fold and 3.6-fold respective increase in the number of colony-forming cells surviving this treatment in the JPV clone 5 cells, while that of an empty or ΔG5 plasmids showed no such increase (Fig. 5A and B). These results indicate that the G5 domain and not ΔG5 has a protective function against HIV-Vpr-induced apoptosis in Jurkat T cells, similar to full-length gelsolin.

3. Discussion

HIV-Vpr causes a rapid dissipation of mitochondrial membrane potential, as well as a mitochondrial release of apoptogenic proteins such as cytochrome *c* or apoptosis inducing factor [6]. The effects of both mitochondrial and cytotoxic Vpr are prevented by Bcl-2, an inhibitor of the permeability transition pore complex (PTPC) [19]. Vpr favors the permeabilization of artificial membranes containing purified PTPC or defined PTPC components such as the adenine nucleotide translocator (ANT) combined with Bax. Again, this effect is prevented by the addition of recombinant Bcl-2. The Vpr carboxyl terminus binds purified ANT, as well as a molecular complex containing ANT and VDAC, another PTPC component. Vpr induces apoptosis via a direct effect on the mitochondrial PTPC [6,19].

Koya et al. previously reported that human cytoplasmic gelsolin is localized not only in the cytosol, but also in the mitochondrial fraction of cells, and that it inhibits the loss of DeltaPsi(m) and cytochrome *c* release from mitochondria in Jurkat cells treated with staurosporine, thapsigargin and protoporphyrin IX [13]. Furthermore, overexpression of gelsolin inhibits the loss of DeltaPsi(m) and cytochrome *c* release from mitochondria and inhibits activation of caspase −3, −8, and −9 in Jurkat cells treated with staurosporine, thapsigargin, and protoporphyrin IX. These effects were corroborated in vitro using recombinant gelsolin protein on isolated rat mitochondria stimulated with calcium, atractyloside, or Bax [13]. The carboxyl-terminal half of gelsolin may also prevent apoptotic mitochondrial changes such as DeltaPsi(m) loss and cytochrome *c* release in isolated mitochondria and inhibit the activity of VDAC on liposomes [20]. Segment 5 of human cytoplasmic gelsolin is the region responsible for inhibition of Amyloid beta-induced cytotoxicity in PC12 rat neuronal cells, in addition to full-length gelsolin [17]. Primary hippocampal neurons cultured from mice lacking gelsolin showed enhanced calcium influx after exposure to glutamate [15]. Whole-cell patch-clamp analyses showed that currents through *N*-methyl-D-aspartate (NMDA) receptors and voltage-dependent calcium channels (VDCC) were enhanced in hippocampal neurons lacking gelsolin. These results suggest roles for gelsolin in events that involve activation of NMDA receptors and VDCC [15]. In this report, we have uncovered another function of gelsolin associated with the ion channel by demonstrating binding to VDAC in mitochondria.

Here we report that gelsolin inhibits HIV-Vpr-induced apoptosis accompanied by the loss of DeltaPsi(m) and cytochrome *c* release from mitochondria in Jurkat T cells. We took advantage of the high transfection efficiency of HEK293T cells to study interactions between VDAC and gelsolin, and demonstrated binding between full-length gelsolin and the G5 segment, but not between other segments and VDAC. Moreover, we demonstrated in HEK293T cells that gelsolin segment 5 shows overlapping, competitive binding of VDAC with HIV-Vpr. These results suggest that gelsolin G5 domain inhibits

HIV-Vpr-induced T-cell apoptosis by blocking binding between Vpr and VDAC. In addition, similar results were obtained in Jurkat cells using full-length gelsolin.

There are reports showing that the presence of antioxidants, such as *N*-acetyl-cysteine, nicotinamide or L-acetyl-carnitine, were able to rescue most of the peripheral blood lymphocytes of subjects with acute HIV syndrome from apoptosis through a protective effect on mitochondria [21]. Additionally, IL-2 and IL-4 produced by peripheral blood mononuclear cells during highly active retroviral therapy provided anti-apoptotic signals that may contribute to an increased survival of T-cells and may thus play a part in long-term immune reconstitution [22]. In this report, we have demonstrated significant protection produced by the G5 gelsolin subunit, but not with other gelsolin domains, from HIV-Vpr-induced apoptotic induction of Jurkat T cells grow on soft agar. These findings suggest a rationale for the use of gelsolin segment 5 protein treatment, in addition to antiviral drugs, in primary HIV infection.

4. Materials and methods

4.1. Plasmid construction

To construct a mammalian expression plasmid with Myc-tagged human cytoplasmic gelsolin (pCI-neo-6xMyc-Gelsolin), the coding sequence was amplified by PCR using LKCG (a kind gift from D. Kwiatkowski of Harvard Medical School) as a template. The resulting PCR products were subcloned into the *EcoRI–SalI* site of the pCI-neo-6xMyc mammalian expression plasmid [23]. Two gelsolin mutants, G5 that encodes segment 5 of human gelsolin (amino acids 516–618) and ΔG5 that lacks the region encoding segment 5, were generated using a PCR-based method and the resulting PCR products were subcloned into pCI-neo-6xMyc, and pCI-neo-6xMyc-G5 and pCI-neo-6xMyc-ΔG5 were prepared, respectively. Human VDAC1 cDNA was obtained by RT-PCR using forward primer (5′-TATGAATTCATGTGTAACACACCAACG-3′) and reverse primer (5′-TATCTCGAGCCTCAAACCACATTAAGC-3′) [24], and the resulting PCR product was subcloned into the *EcoRI–SalI* site of pCI-neo-3xT7 as described previously [23], and pCI-neo-3XT7-VDAC was constructed. Vpr sequence derived from the plasmid vector pME18Neo-F(lag)Vpr containing HIV-1-Vpr [5] (a generous gift from Dr. Aida, Retrovirus Research Unit, RIKEN, Wako, Saitama, Japan) and the Flag tag-Vpr was subcloned into plasmid vector pTRE2-Hyg (Clontech) to generate the pTRE2-Hyg-Vpr plasmid.

4.2. Cell culture and establishment of stable cell lines

A lymphoblastoid T-cell line Jurkat (parental Jurkat: JP), and its stable clones transfected with human cytoplasmic gelsolin plasmid LKCG (JGF clone 5) or with the control plasmid LK444 (a kind gift from P. Gunning) (JNF clone 2), were maintained in RPMI 1640 medium containing 10% fetal calf serum (FCS) (Gibco BRL, Gaithersburg, MD) as described previously [12]. HEK293T cells was maintained in Dulbecco's modified Eagle's medium (DMEM) containing 10% FCS. All cells were cultured at 37 °C in a 5% CO2 humidified atmosphere.

The Tet-on system (Clontech, Mountain View, CA) was used to obtain stable cell lines that express HIV-1-Vpr. JP, JNF and JGF (1×10^6) were transfected with 2 μg of regulator plasmid pTracer-CMV2-Tet-on containing reverse tetracycline-controlled transactivator (rtTA), which interacts with the inducible promoter in the presence of tetracycline or analogues as Dox and activates transcription, and 12 μg/ml of SuperFect transfection reagent (Qiagen, Tokyo) according to the manufacturer's instructions. Each transfectant was selected in the presence of 0.8 mg/ml zeocin (Invitrogen, Carlsbad, CA). To select clones with high expression of rtTA, total RNA was isolated from JP-Tet-on JNF-Tet-on and JGF-Tet-on cell lines with extraction reagent (TRIzol, Invitrogen). The RT-PCR was performed with 1 μg of RNA from each sample, with reverse transcriptase (Superscript II; Gibco BRL, Carlsbad, CA) and random primer. The reverse transcript was incubated with Taq-polymerase and primers rtTA forward (5′-GAGGTCGGAATCGAAGGTTT-3′), which matches the coding strand of rtTA at positions 55–74, and rtTA reverse (5′-TCGTAATAATGGCGGCATAC-3′), which matches the reverse strand of rtTA at positions 513–522, as described previously [24], for 35 cycles (denaturing: 30 s 95 °C; annealing: 30 s 55 °C; elongation: 90 s 72 °C), followed by a 7 min 72 °C extension. Electrophoresis of PCR-products was performed on a 1% agarose gel containing ethidium bromide. JP-Tet-on JNF-Tet-on and JGF-Tet-on cell lines that expressed higher rtTA were selected. Next, the selected Tet-on cell lines, JP-Tet-on JNF-Tet-on and JGF-Tet-on, were transfected with pTRE2-Hyg-Vpr and each transfectant (JPV clone 5; JNFV clones 3, 4, 7; JGFV clones 2, 8, 9) was further selected in the presence of 400 μg/ml Hygromycin (Wako, Osaka, Japan). To investigate clones with high expression of HIV-Vpr, each Tet-on cell line was treated with 2 μg/ml of Dox and the expression of HIV-Vpr confirmed by IB.

4.3. Immunoblotting analysis

Total cells were extracted in SDS sample buffer (40 mM Tris–HCl, pH 7.4, 5% 2ME, 2% SDS, 0.05% bromphenol blue). Cell lysates were analyzed by SDS–polyacrylamide gel electrophoresis and IB as described previously [13,22] using monoclonal anti-human gelsolin (GS-2C4, Sigma), monoclonal anti-cytochrome *c* (Pharmingen, Mississauga, ON, Canada), anti-Myc monoclonal antibody (Clontech), anti-T7 tag monoclonal antibody (Novagen, San Diego, CA), monoclonal anti-FLAG (M2) antibody (Sigma), monoclonal anti-VDAC (Sigma) and anti-β-actin monoclonal antibody (Chemicon, Temecula, CA). The bound primary antibodies were incubated with peroxidase-conjugated anti-mouse IgG+M (Jackson ImmunoResearch Lab., West Grove, PA) and detected by ECL Western blotting detection reagents (Amersham Biosciences). Band images were detected by a LAS 1000 mini system (Fuji Film, Kanagawa, Japan).

4.4. Assays for cell viability and mitochondrial functions

Cell viability and apoptotic cell death were assessed using Hoechst 33342 (Sigma, St. Louis, MO) and propidium iodide (PI) staining, MMP assayed by the addition of Rhodamine 123 to the culture medium, and cytochrome *c* release from mitochondria into the cytosol of Jurkat cells evaluated by SDS–polyacrylamide gel electrophoresis followed by IB of the cytosolic fraction, as previously described [13]. For cell viability and mitochondrial functions, JPV, JNFV, and JGFV cell lines were examined at 24, 48 or 72 h and 72 h in the presence or absence of 2 μg/ml Dox, respectively.

4.5. Co-immunoprecipitation analysis

HEK293T cells were transiently transfected with expression plasmid as indicated. Forty-eight hours after transfection, the cells were washed with ice-cold Tris-buffered saline (TBS) and harvested. The cells were then lyzed with immunoprecipitation (IP) buffer containing 50 mm Tris–HCl (pH 7.5), 150 mm NaCl, 0.5% Triton X-100, 10% glycerol, 0.1 mM PMSF, 10 μg/ml aprotinin, 1 μg/ml chymostatin, 1 μg/ml leupeptin, and 1 μg/ml pepstatin. The lysates were incubated on ice for 30 min, and the cell debris was removed by centrifugation at 13000*g* for 20 min. The resulting supernatants were pretreated with 20 μl Protein G-Sepharose beads (Roche,Tokyo, Japan) at 4 °C for 1 h and was then incubated with 2 μg anti-T7 tag or anti-Myc monoclonal antibody and 20 μl Protein G-Sepharose beads at 4 °C for 2 h. The immunocomplex that was produced was washed five times with IP buffer. SDS-sample buffer was added to the beads, and the samples were boiled. The immunoprecipitates and the cell lysates were subjected to IB analysis. For JPFV, JNFV and JGFV cell lines, 48 h after treatment with Dox, the cell lysates were then incubated with 2 μg anti-VDAC monoclonal antibody under the same conditions as previously mentioned.

4.6. Clonogenic assay

Clonogenic analysis was performed as described previously [25]. Using electroporation, 1×10^7 JPV clone 5 cells were transfected with expression plasmids: pCI-neo-6xMyc, pCI-neo-6xMyc-Gelsolin, pCI-neo-6xMyc-G5 or pCI-neo-6xMyc-ΔG5. Forty-eight hours after transfection, both 2 μg/ml Dox and 1 mg/ml neomycin were added to the medium. All cells harvested from each plate were suspended in 5 ml of 0.5% agarose containing 20% FCS medium and then plated on the top of 5 ml of 1% semi-solidified agarose (Nacalai Tesque Inc. Kyoto. Japan) with the same medium in 10 cm plates. For each

vector control, full-length gelsolin, G5 and ΔG5 clones, triplicate plates were used. The plates were incubated for 2 weeks at 37 °C in the presence of 5% CO2 in an incubator. They were then stained with 0.5 ml of 0.005% Crystal Violet for more than 1 h. Colonies grown on agarose were counted using a microscope.

4.7. Statistical analysis

The data shown represent mean values of at least three different experiments, expressed as mean ± S.E. Student's *t* test was used to compare the data, and a *P* value of less than 0.05 was considered statistically significant.

Acknowledgments: This work was supported by a grant-in-aid from the Health and Labor Sciences Research Grant (research into Human Genome, Tissue Engineering) H17-Saisei-12 (J.R.M.). We also thank Drs. N. Kuzumaki and H. Shimizu for helpful discussion.

References

[1] Roshal, M., Zhu, Y. and Planelles, V. (2001) Apoptosis in AIDS. Apoptosis 6, 103–116.
[2] Bukrinsky, M. and Adzhubei, A. (1999) Viral protein R of HIV-1. Reviews in Medical Virology 9, 39–49.
[3] Ayyavoo, V., Mahalingam, S., Rafaeli, Y., Kudchodkar, S., Chang, D., Nagashunmugam, T., Williams, W.V. and Weiner, D.B. (1997) HIV-1 viral protein R (Vpr) regulates viral replication and cellular proliferation in T cells and monocytoid cells in vitro. Journal of Leukocyte Biology 62, 93–99.
[4] Emerman, M. (1996) HIV-1, Vpr and the cell cycle. Current Biology 6, 1096–1103.
[5] Nishizawa, M., Kamata, M., Mojin, T., Nakai, Y. and Aida, Y. (2000) Induction of apoptosis by the Vpr protein of human immunodeficiency virus type 1 occurs independently of G(2) arrest of the cell cycle. Virology 276, 16–26.
[6] Jacotot, E., Ravagnan, L., Loeffler, M., Ferri, K.F., Vieira, H.L., Zamzami, N., Costantini, P., Druillennec, S., Hoebeke, J., Briand, J.P., Irinopoulou, T., Daugas, E., Susin, S.A., Cointe, D., Xie, Z.H., Reed, J.C., Roques, B.P. and Kroemer, G. (2000) The HIV-1 viral protein R induces apoptosis via a direct effect on the mitochondrial permeability transition pore. J. Exp. Med. 191, 33–46.
[7] Basanez, G. and Zimmerberg, J. (2001) HIV and apoptosis death and the mitochondrion. J. Exp. Med. 193, F11–F14.
[8] Kwiatkowski, D.J., Stossel, T.P., Orkin, S.H., Mole, J.E., Colten, H.R. and Yin, H.L. (1986) Plasma and cytoplasmic gelsolins are encoded by a single gene and contain a duplicated actin-binding domain. Nature 323, 455–458.
[9] Sun, H.Q., Yamamoto, M., Mejillano, M. and Yin, H.L. (1999) Gelsolin, a multifunctional actin regulatory protein. J. Biol. Chem. 274, 33179–33182.
[10] Kothakota, S., Azuma, T., Reinhard, C., Klippel, A., Tang, J., Chu, K., McGarry, T.J., Kirschner, M.W., Koths, K., Kwiatkowski, D.J. and Williams, L.T. (1997) Caspase-3-generated fragment of gelsolin: effector of morphological change in apoptosis. Science 278, 294–298.
[11] Burtnick, L.D., Urosev, D., Irobi, E., Narayan, K. and Robinson, R.C. (2004) Structure of the N-terminal half of gelsolin bound to actin: roles in severing, apoptosis and FAF. EMBO J. 23, 2713–2722.
[12] Ohtsu, M., Sakai, N., Fujita, H., Kashiwagi, M., Gasa, S., Shimizu, S., Eguchi, Y., Tsujimoto, Y., Sakiyama, Y., Kobayashi, K. and Kuzumaki, N. (1997) Inhibition of apoptosis by the actin-regulatory protein gelsolin. EMBO J. 16, 4650–4656.
[13] Koya, R.C., Fujita, H., Shimizu, S., Ohtsu, M., Takimoto, T., Tsujimoto, Y. and Kuzumaki, N. (2000) Gelsolin inhibits apoptosis by blocking mitochondrial membrane potential loss and cytochrome *c* release. J. Biol. Chem. 275, 15343–15349.
[14] Klampfer, L., Huang, J., Sasazuki, T., Shirasawa, S. and Augenlicht, L. (2004) Oncogenic Ras promotes butyrate-induced apoptosis through inhibition of gelsolin expression. J. Biol. Chem. 279, 36680–36688, (Journal Article).
[15] Furukawa, K., Fu, W., Li, Y., Witke, W., Kwiatkowski, D.J. and Mattson, M.P. (1997) The Actin-severing protein gelsolin modulates calcium channel and NMDA receptor activities and vulnerability to excitotoxicity in hippocampal neurons. J. Neurosci. 17, 8178–8186.
[16] Harms, C., Bosel, J., Lautenschlager, M., Harms, U., Braun, J.S., Hortnagl, H., Dirnagl, U., Kwiatkowski, D.J., Fink, K. and Endres, M. (2004) Neuronal gelsolin prevents apoptosis by enhancing actin depolymerization. Mol. Cell. Neurosci. 25, 69–82.
[17] Qiao, H., Koya, R.C., Nakagawa, K., Tanaka, H., Fujita, H., Takimoto, M. and Kuzumaki, N. (2005) Inhibition of Alzheimer's amyloid-β peptide-induced reduction of mitochondrial membrane potential and neurotoxicity by gelsolin. Neurobiology of Aging 26, 849–855.
[18] Orth, P., Schnappinger, D., Hillen, W., Saenger, W. and Hinrichs, W. (2000) Structural basis of gene regulation by the tetracycline inducible Tet repressor-operator system. Nat. Struct. Biol. 7, 215–219.
[19] Jacotot, E., Ferri, K.F., El Hamel, C., Brenner, C., Druillennec, S., Hoebeke, J., Rustin, P., Metivier, D., Lenoir, C., Geuskens, M., Vieira, H.L., Loeffler, M., Belzacq, A.S., Briand, J.P., Zamzami, N., Edelman, L., Xie, Z.H., Reed, J.C., Roques, B.P. and Kroemer, G. (2001) Control of mitochondrial membrane permeabilization by adenine nucleotide translocator interacting with HIV-1 viral protein R and Bcl-2. J. Exp. Med. 193, 509–519.
[20] Kusano, H., Shimizu, S., Koya, R.C., Fujita, H., Kamada, S., Kuzumaki, N. and Tsujimoto, Y. (2000) Human gelsolin prevents apoptosis by inhibiting apoptotic mitochondrial changes via closing VDAC. Oncogene 19, 4807–4814.
[21] Andrea, C., Cristina, M., Nicola, M., Vanni, B., Anna, S., Bruno, D.R. and Claudio, F. (1997) Mitochondria alterations and dramatic tendency to undergo apoptosis in peripheral blood lymphocytes during acute HIV syndrome. AIDS 11, 19–26.
[22] Ensoli, F., Fiorelli, V., De Cristofaro, M., Collacchi, B., Santini Muratori, D., Alario, C., Sacco, G., Iebba, F. and Aiuti, F. (2002) Endogenous cytokine production protects T cells from spontaneous apoptosis during highly active antiretroviral therapy. HIV Medicine 3, 105–117.
[23] Nakagawa, K. and Kuzumaki, N. (2005) Transcriptional activity of megakaryoblastic leukemia 1 (MKL1) is repressed by SUMO modification. Genes to Cells 10, 835–850.
[24] Mao, M., Fu, G., Wu, J.S., Zhang, Q.H., Zhou, J., Kan, L.X., Huang, Q.H., He, K.L., Gu, B.W., Han, Z.G., Shen, Y., Gu, J., Yu, Y.P., Xu, S.H., Wang, Y., Chen, S.J. and Chen, Z. (1998) Identification of genes expressed in human CD34(+) hematopoietic stem/progenitor cells by expressed sequence tags and efficient full-length cDNA cloning. Proc. Natl. Acad. Sci. USA 95, 8175–8180.
[25] Longthorne, V.L. and Williams, G.T. (1997) Caspase activity is required for commitment to Fas-mediated apoptosis. EMBO J. 16, 3805–3812.

nature medicine

Humanization of autoantigen

Wataru Nishie[1,3], Daisuke Sawamura[1,3], Maki Goto[1], Kei Ito[1], Akihiko Shibaki[1], James R McMillan[1], Kaori Sakai[1], Hideki Nakamura[1], Edit Olasz[2], Kim B Yancey[2], Masashi Akiyama[1] & Hiroshi Shimizu[1]

Transmissibility of characteristic lesions to experimental animals may help us understand the pathomechanism of human autoimmune disease. Here we show that human autoimmune disease can be reproduced using genetically engineered model mice. Bullous pemphigoid (BP) is the most common serious autoimmune blistering skin disease, with a considerable body of indirect evidence indicating that the underlying autoantigen is collagen XVII (COL17). Passive transfer of human BP autoantibodies into mice does not induce skin lesions, probably because of differences between humans and mice in the amino acid sequence of the COL17 pathogenic epitope. We injected human BP autoantibody into *Col17*-knockout mice rescued by the human ortholog. This resulted in BP-like skin lesions and a human disease phenotype. Humanization of autoantigens is a new approach to the study of human autoimmune diseases.

Evolution of a complex immune system in mammals can paradoxically lead to an increased likelihood of autoimmune disease, which affects approximately 5% of the general population[1]. The immune system comprises two evolutionarily different responses: innate immunity and adaptive immunity. Vertebrates are capable of both adaptive and innate immunity, which is common to all metazoans, and are consequently exposed to autoimmune diseases—in which an aberrant, adaptive immune system recognizes a self-component as an autoantigen.

To understand the pathogenesis of these diseases and to develop new therapies, animal models corresponding to human autoimmune diseases are essential[2,3]. A small number of experimental animal models of autoimmune diseases have been generated by the passive transfer of autoantibodies from individuals[4,5], but this approach has not been universally successful because of limited interspecies recognition of the autoantigen by the adaptive immune system. In reality, most animal models that reflect human autoimmune diseases have been identified from spontaneously arising diseases or have been generated by repeated immunization using host candidate autoantigens[2,3].

Although these animal models may develop certain aspects of human autoimmune diseases, there is as yet no reliable method to produce models that identically and faithfully reproduce human autoimmune disorders. Recently, transgenic mice expressing disease-associated human *HLA* alleles and T-cell receptors have been generated, which have the potential to provide further insight into the pathogenesis of many diseases[2,3,6,7]. Conversely, few advances have been made in humanizing autoantigens in animals.

Our study therefore focused on this approach in BP, the most common antibody-mediated autoimmune blistering skin disease. Although the sera of individuals with bulbus pemphigoid (BP) are known to contain autoantibodies to the collagen XVII (COL17) autoantigen, the pathogenicity of COL17 autoantibodies has not been unequivocally proven as previous passive transfer experiments have failed[8,9]. In the native COL17 epidermal protein, the pathogenic epitope is restricted to the noncollagenous 16th-A (NC16A) domain[10], which shows distinct diversity among different species[8,9]. Here, to assess the direct pathogenicity of human BP autoantibodies in a mouse model, we humanized the mouse BP autoantigen. Furthermore, we used this new mouse to demonstrate that COL17 decoy peptides block the pathogenic activity of BP-IgG *in vivo*.

RESULTS

Generation of COL17-humanized ($COL17^{m-/-,h+}$) mice

We first generated *Col17*-knockout ($COL17^{m-/-}$) mice, in which the phenotypic features closely resembled the human disease non-Herlitz epidermolysis bullosa (OMIM: 226650) caused by null mutations in the *COL17A1* gene (**Fig. 1** and refs. 11–13). When $COL17^{m-/-}$ mice were born, blisters and erosions at sites of trauma were easily created by applying mild friction, and some pups exhibited spontaneous blister formation on their paws (**Fig. 1c**). Other characteristic findings seen in adult $COL17^{m-/-}$ mice were genital erosions, hemorrhagic blisters around the digits, and diffuse, nonpigmented hair growth associated with hair loss (**Fig. 1d,e**). $COL17^{m-/-}$ mice showed growth retardation compared with wild-type littermates, and most $COL17^{m-/-}$ mice died within 2 weeks of birth. Mortality rates of the $COL17^{m-/-}$ and wild-type littermates at 8 weeks were 80.1% and 4.0%, respectively (**Supplementary Fig. 1** online). $COL17^{m-/-}$ mice skin showed subepidermal blistering (**Fig. 1f**) associated with a lack of collagen XVII immunostaining (**Fig. 1g**), and ultrastructurally showed small and poorly formed hemidesmosomes (**Fig. 1h**) lacking prominent inner (IP) and outer (OP) plaques and keratin filament insertion compared to controls.

Next, we rescued $COL17^{m-/-}$ mice by mating them with C57BL/6Ncr mice expressing human COL17 under the control of a human keratin 14 promoter ($COL17^{h+}$) (data not shown). After crossing heterozygote $COL17^{m-/+}$ mice and human COL17 transgenic

[1]Department of Dermatology, Hokkaido University Graduate School of Medicine, Sapporo 060-8638, Japan. [2]Department of Dermatology, Medical College of Wisconsin, 8701 Watertown Plank Road, Milwaukee, Wisconsin 53226, USA. [3]These authors contributed equally to this work. Correspondence should be addressed to H.S. (shimizu@med.hokudai.ac.jp).

Received 14 August 2006; accepted 26 September 2006; published online 25 February 2007; doi:10.1038/nm1496

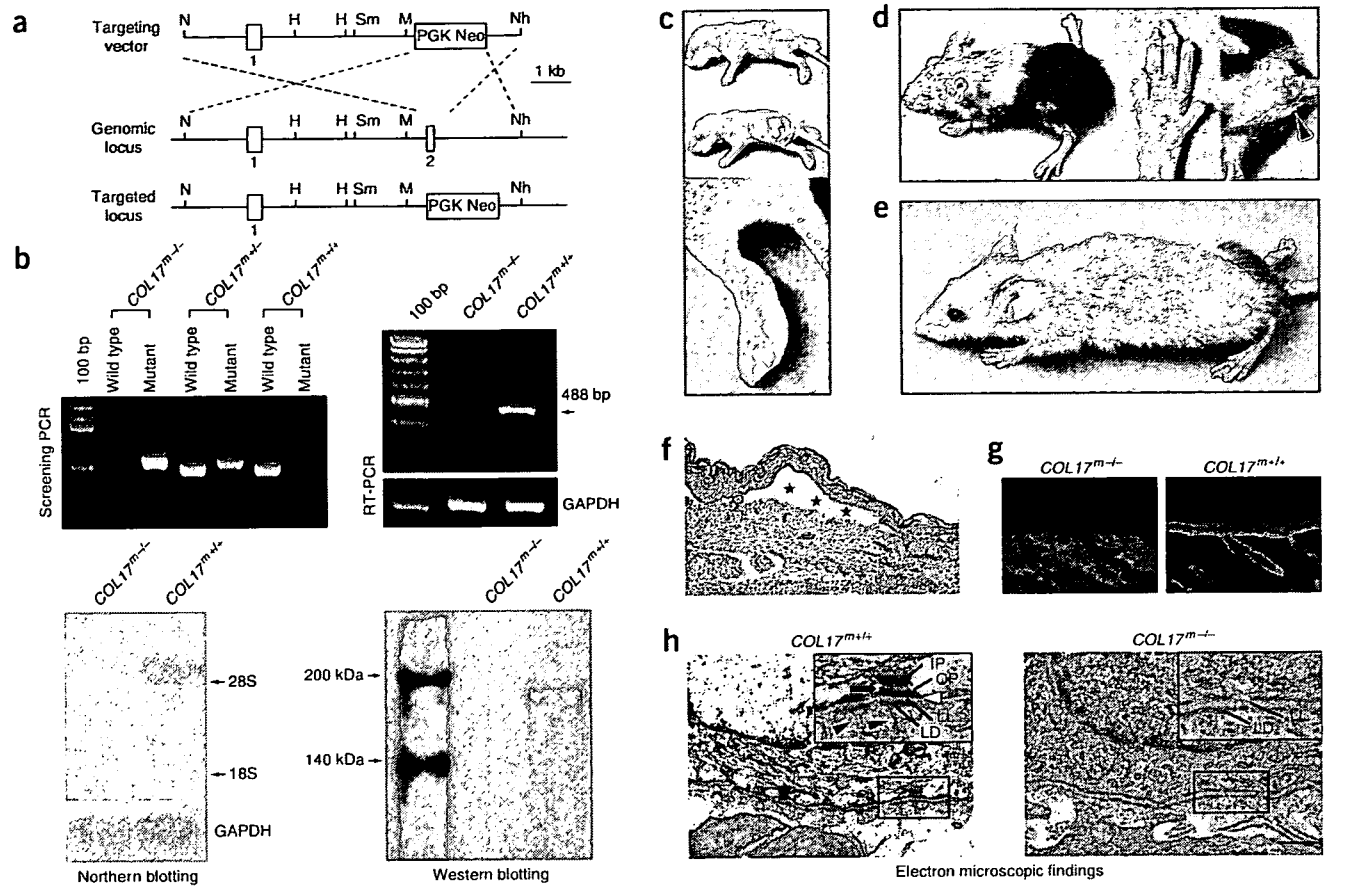

Figure 1 Generation of *COL17*$^{m-/-}$ mice. (**a**) The targeting vector was constructed by disrupting exon 2. (**b**) PCR reaction amplified a 562-bp mutant band, and a 496-bp fragment corresponding to the wild-type genomic *Col17* DNA. RT and subsequent PCR reactions, northern and western blotting showed definite disruption of *COL17* mRNA and its transcript in *COL17*$^{m-/-}$ mouse keratinocytes. These findings were characteristic of *COL17*$^{m-/-}$ mice. (**c**) Epidermal detachment after gentle friction (arrows), and blister development on the paw. (**d**) Eight-week-old *COL17*$^{m-/-}$ mouse. Note the white hair around the face and head, small hemorrhagic blisters and scar formation on the paw and digits, nail loss, and erosions within the genital area (arrowhead). (**e**) White hair growth over the entire body of a 12-week old *COL17*$^{m-/-}$ mouse. (**f**) Light microscopy revealed blister formation beneath the epidermis of *COL17*$^{m-/-}$ mouse skin (stars). (**g**) Immunofluorescence study of *COL17*$^{m-/-}$ and wild-type mice skin. COL17 did not show any immunoreactivity (mNC16A antibody) along the dermal-epidermal junction in the *COL17*$^{m-/-}$ mice. (**h**) Electron microscopy findings. In wild-type skin, hemidesmosomes were composed of prominent inner plaques (IP), outer plaques (OP) and sub-basal dense plates (arrow). Anchoring filaments (white arrowhead) spanned the lamina lucida (LL), and anchoring fibrils (black arrowheads) extended from lamina densa (LD) to the papillary dermis. In *COL17*$^{m-/-}$ skin, there were a reduced number of hypoplastic (small) hemidesmosomal inner and outer attachment plaques with poor keratin filament attachment and less prominent anchoring filaments, whereas anchoring fibrils and the lamina densa (LD) were both well preserved. Scale bar, 300 nm.

(*COL17*$^{m+/+,h+}$) mice, we generated rescued COL17-humanized (*COL17*$^{m-/-,h+}$) mice (**Fig. 2a–c**). Notably, rescued COL17-humanized mice showed none of the abnormal manifestations seen in *COL17*$^{m-/-}$ mice (**Fig. 2a** and **Supplementary Fig. 1**). The rescued mice were able to reproduce, in spite of the fact that the original *COL17*$^{m-/-}$ mice were unable to multiply.

IgG transfer from BP patients to COL17-humanized mice

We then performed a passive transfer study using pathogenic IgG from individuals with BP. Preliminary studies in human COL17 transgenic (*COL17*$^{m+/+,h+}$) mice did not show skin detachment (data not shown); therefore we studied neonatal COL17-humanized mice instead.

The COL17-humanized mice received intraperitoneal injections of both total and affinity-purified IgG directed against COL17, and developed diffuse erythema and a positive Nikolsky sign (epidermal separation elicited by gentle skin friction) at 48 h after injection (**Fig. 2d** and **Table 1**). Histopathologic studies of lesional skin revealed a separation between the epidermis and the dermis, and an inflammatory cell infiltrate including neutrophils and lymphocytes (**Fig. 2e**). Direct immunofluorescence studies revealed a linear deposition of human IgG along the dermal-epidermal junction (**Fig. 2f**). Electron microscopic findings showed dermal-epidermal separation in the lamina lucida between the plasma membrane of basal keratinocytes and the lamina densa (**Fig. 2g**). All these findings are consistent with, and precisely recapitulate, human BP skin lesions[14], thus confirming that these mice are a good model for human BP disease. We demonstrate that this disease is initiated by an interaction between human BP autoantibodies and the human COL17 adhesion protein.

Recombinant peptide epitope decoy therapy

Finally, using this system, we evaluated the efficiency of a new approach to BP therapy. We synthesized six different short peptides

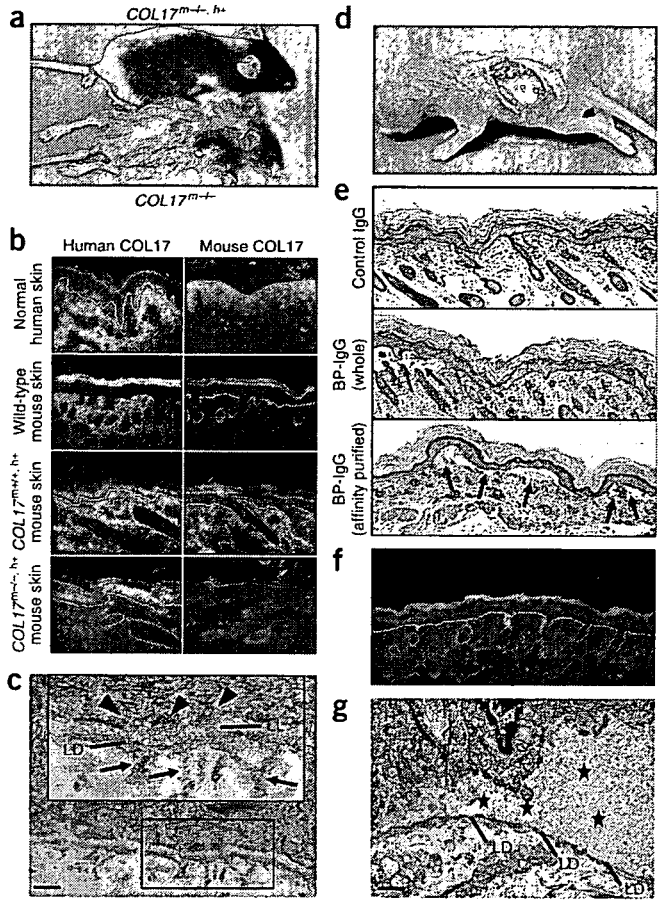

Figure 2 Phenotype, immunohistochemistry and histology of the humanized model mice. (**a**) *COL17*$^{m-/-}$ mouse and rescued COL17-humanized mouse (*COL17*$^{m-/-,h+}$). Compared to the *COL17*$^{m-/-}$ mouse, the COL17-humanized mouse showed no abnormal clinical manifestations. (**b**) Immunofluorescence studies using antibody to human COL17 and mouse COL17 showed that in human skin, only human COL17 was positively stained, whereas mouse COL17 did not stain. By contrast, mouse COL17 was positively stained only in mouse skin. In human COL17 transgenic (*COL17*$^{m+/+,h+}$) mice skin, both human COL17 and mouse COL17 were positively stained. Note that in the rescued COL17-humanized mice skin, mouse COL17 was absent whereas human COL17 was present. (**c**) Electron microscopy findings from the rescued COL17-humanized mice skin. Note the distinct, normal-looking hemidesmosomes with clear keratin filament attachment (arrowheads) adjacent to the lamina lucida (LL), lamina densa (LD) and anchoring fibrils (arrows). Scale bar, 200 nm. (**d**) COL17-humanized mouse injected with pathogenic IgG showed diffuse erythema and the epidermis was frequently detached from the dermis. (**e**) Histological findings in IgG-injected mice skin. There were no abnormal findings in control mice skin, whereas mice skin injected with the whole IgG fraction showed subepidermal blisters. Furthermore, mice skin injected with COL17 affinity-purified IgG showed a greater degree of subepidermal blistering with inflammatory cells. (**f**) Direct immunofluorescence microscopy showed linear IgG deposition along the dermal-epidermal junction. (**g**) Electron microscopy of rescued mice skin injected with BP-IgG revealed skin separation as well as putative blisters (stars) developing within the lamina lucida overlying the the lamina densa (LD). Scale bar, 1 μm.

overlapping a number of antigenic COL17 NC16A microdomains (**Fig. 3a**). *In vitro* immune-adsorption studies showed that a recombinant peptide composed of 77 amino acids (R1) most efficiently suppressed the BP antibody index (defined as follows: index = (optical density (OD) of tested serum − OD of negative control)/(OD of positive control − OD of negative control) × 100; all index values against BP antibodies were measured by ELISA using COL17 NC16A domain peptide; see Methods) from BP sera (**Fig. 3b** and **Supplementary Methods** online). Furthermore, we found that the suppression efficacy of R1 was increased after fusion of glutathione *S*-transferase (GST) (**Fig. 3b**). This R1-GST peptide reduced index values of BP-IgG in a dose-dependent manner in an *in vitro* binding assay (**Fig. 3c**).

For *in vivo* studies, after intraperitoneal injection of 1 mg/g (body weight) total IgG from individuals with BP, we treated COL17-humanized mice with R1-GST peptide (total dose of 600 μg, injected subcutaneously). This resulted in a marked reduction in blister formation (specifically, no blisters or skin fragility in 16 out of 17 mice), in contrast to controls treated with GST alone (extensive blisters in 12 of 16 mice) (**Fig. 3d** and **Table 2**). Histopathologically, mouse skin treated with R1-GST showed no subepidermal blister formation, whereas distinctive blister formation developed in control mouse skin (**Fig. 3d**). Direct immunofluorescence studies showed substantially reduced human IgG staining along the dermal-epidermal junction in the group treated with recombinant protein compared to the control group, indicating that the R1-GST peptide can efficiently neutralize pathogenic IgG *in vivo* (**Fig. 3d**). BP antibody index value was also significantly decreased in the treated group (**Fig. 3e**, $n = 15$, $P <$ 0.01). We observed no adverse reactions, such as anaphylaxis or dermatitis, to the peptide treatments.

DISCUSSION

Here we succeeded in generating a *COL17*$^{m-/-}$ mouse, which represents a human disease model of non-Herlitz junctional epidermolysis bullosa[11–13]. We also generated COL17-humanized (*COL17*$^{m-/-,h+}$) mice with a normal appearance, clearly showing that the transgenic epidermal COL17 product that originated from the transfected *COL17* cDNA is able to abolish the clinical features of the *COL17*$^{m-/-}$ mouse. This supports the previously proposed notion that genetic diseases with defective epidermally expressed genes, such as those in the epidermolysis bullosa group of diseases, can be treated by gene therapy using an appropriate cDNA, even one from another species.

The potential pathogenic role of COL17 has been supported in an experimental mouse passive transfer model using rabbit IgG directed against the murine homolog of the immunodominant epitope of human COL17 (ref. 9). Indeed, many previous attempts have been made to try to directly confirm the pathogenicity of human COL17 BP autoantibodies. Of note, a new model was developed by administering IgG fractions from individuals with BP into human skin grafted onto adult severe combined immunodeficient (SCID) mice. No blister formation was observed, however, although human IgG and mouse C3 were both deposited at the epidermal basement membrane zone of the grafted human skin[15].

Here we were able to generate BP lesions in experimental mice using autoantibodies from human BP patients. Several factors have contributed to the success of this model system. First, rescued COL17-humanized mice possess a functional, humanized COL17 protein that is faithfully recognized by IgG autoantibodies from individuals with BP. Second, we performed this passive transfer study using neonatal mice, which might have resulted in a higher index value of circulating IgG in the host mice (because of smaller blood and body volumes). Third, we observed no epidermal detachment in human COL17 transgenic (*COL17*$^{m+/+,h+}$) mice that had been given pathogenic BP-IgG. The transgenic mice possessed both human and mouse COL17, and the inflammatory process induced by BP-IgG in this model might

Table 1 Characteristics of serum and IgG from BP patients showing the extent of disease in neonatal mice

	Serum from BP patients				Passive transfer of IgG into COL17-humanized mice	
Patient	IIF titer human skin	IIF titer mouse skin	BP180 ELISA index value	BP230 ELISA index value	Dose of IgG or COL17-affinity IgG (mg per g body weight)	Skin detachment
1	×320	Neg	171.4	Neg	2	5/6
					1	7/7
					0.5	3/6
					0.25	0/7
					0.05	5/5
2	×320	Neg	162.5	27.06	2	7/7
					1	7/7
					0.5	3/5
					0.25	2/6
					0.05	5/5
3	×320	Neg	142.4	Neg	2	5/5
					1	5/5
					0.5	3/6
					0.25	2/6
					0.05	5/5
4	×320	Neg	184.4	Neg	2	5/6
					1	6/8
					0.5	5/7
					0.25	4/5
					0.05	ND
5	×40	Neg	125.5	Neg	2	5/5
					1	5/5
					0.5	5/6
					0.25	2/5
					0.05	ND
Healthy control ($n = 5$)	Neg	Neg	Neg	Neg	2	0/5
					1	0/5
					0.5	0/5
					0.25	0/5
					0.05	0/5

The COL17-humanized mice that were injected intraperitoneally with whole IgG fractions and with COL17 affinity-purified (underlined) IgG fraction developed distinct skin fragility (positive Nikolsky sign) at 48 h. In contrast, control IgG from healthy volunteers resulted in no detectable abnormal skin lesions ($n = 5$, all mice were injected with total IgG because COL17 affinity IgG was not obtainable). Neg, negative; ND, not done.

have been insufficient for blistering or disrupting mouse COL17 dermal-epidermal adhesion. In fact, the BP-IgG–treated COL17-humanized mice developed the blistering disease because they expressed only the human COL17 and not the mouse antigen. Last, our study showed that COL17-humanized mice have a normal mouse immune system, in contrast to previous findings in SCID mice. We showed a direct induction of human BP lesions in COL17-humanized mice, which provides strong and irrefutable evidence that human BP autoantibodies directly cause subepidermal blisters. Humanization of autoantigens in model animals therefore represents a powerful technical approach capable of improving our understanding of this and other autoimmune diseases.

In addition, we showed that a therapeutic challenge with a recombinant peptide sequence containing the BP pathogenic epitope as a decoy markedly inhibited the formation of BP skin lesions and decreased disease severity. One or more epitopes for BP autoantibodies are clustered within a limited area of the NC16A domain[10]. This domain resides within the COL17 ectodomain, in a region that is closest to the transmembrane domain and where circulating autoantibodies have easy access[16]. We used this known characteristic of BP antibodies to design an effective 'trap' for the BP autoantibodies. We did this by synthesizing a short recombinant peptide harboring the pathogenic BP epitope sequence, which is capable of acting as a decoy. Moreover, we found that the capacity of the R1 antigenic peptide to bind antibodies to NC16A BP-IgG was increased after coupling with GST. This is consistent with a previous report showing that COL17 NC16A domain peptides obtain a more beneficial conformation, including α-helix and β-turn, after linking with GST, in terms of a higher ligand affinity for the substrate (as determined by ELISA; ref. 17). Here we showed that this epitope decoy strategy has potential for the treatment of antibody-mediated autoimmune diseases in clinical practice. Overall, we believe that the new mouse model and the technical approach we have followed provide a strong basis for future studies that can provide new insight into the pathomechanisms and therapy of human autoimmune diseases.

METHODS

Generation of *COL17*$^{m-/-}$ mouse. We cloned a 14.7-kb mouse genomic DNA Col17 fragment from the mouse 129Sv/Ev genomic library (Stratagene). We subcloned a 11.5-kb *Nhe*I to *Not*I fragment to make the targeting vector. We inserted the PGK/Neo cassette between 6 bp upstream of the ATG start codon in exon 2 and 1.2 kb downstream in intron 2. We transfected the targeting vector by electroporation into 129 Sv/Ev embryonic stem cells, then microinjected the correctly targeted embryonic stem cell line into blastocysts

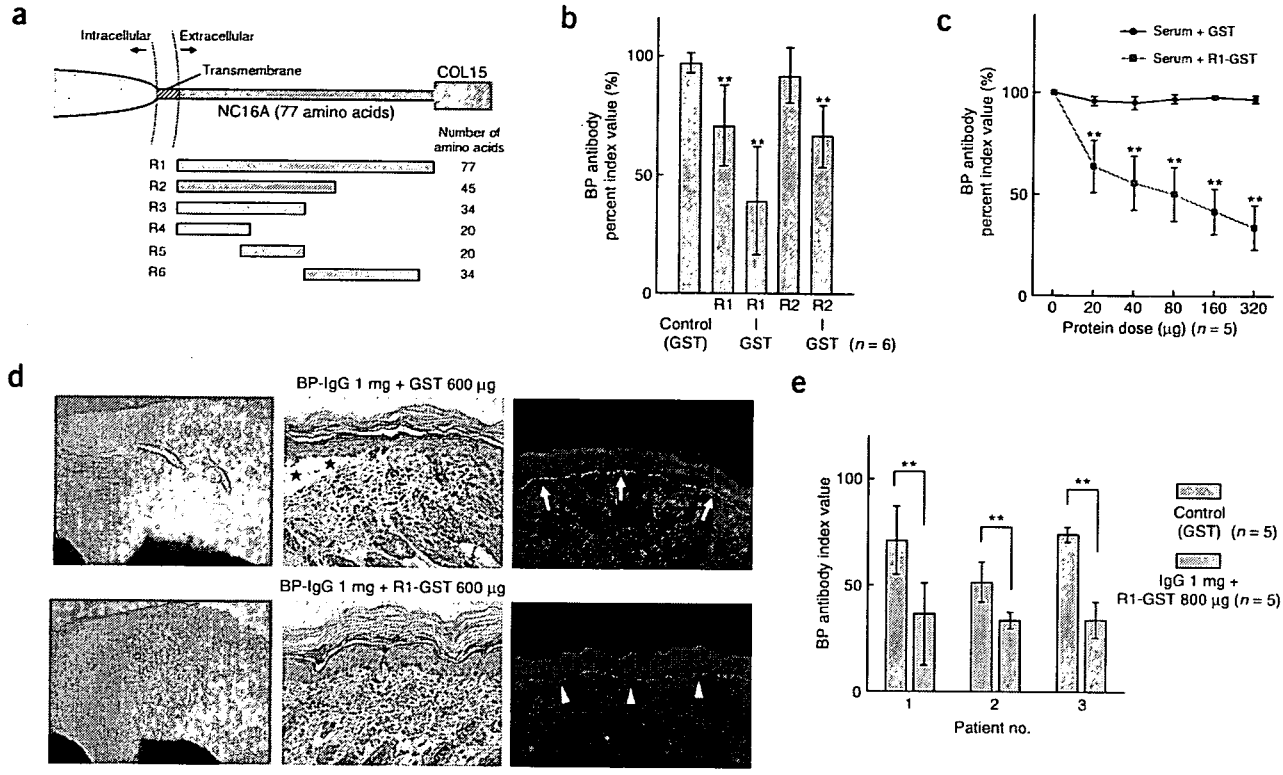

Figure 3 BP disease response to therapeutic decoy peptides. (**a**) Schematic of the antigenic epitope of COL17, NC16A domain and therapeutic recombinant proteins. The 77 amino-acid-long NC16A domain is located between the 15th extracellular collagenous domain from the C terminus (COL15) and transmembrane residues. R1 to R6 refers to the recombinant decoy peptides that are complementary to different portions and different lengths of the corresponding NC16A domain. (**b**) R1-GST suppressed BP autoantibody index values most effectively in an *in vitro* immunoadsorption study ($n = 6$, $P = 0.0038$). (**c**) R1-GST protein suppressed BP antibody index values in a dose-dependent manner, whereas control GST protein had no therapeutic effect ($n = 5$). (**d**) A control COL17-humanized mouse injected with pathogenic BP autoantibody and the GST peptide developed clinical and histological skin detachment (stars), associated with IgG deposits at the basement membrane zone (arrows). In contrast, a mouse treated with the R1-GST did not show these clinical or histological characterstics, and IgG deposition along the dermal-epidermal junction was reduced (arrowheads). (**e**) BP autoantibody index values (as assessed by ELISA) were also significantly reduced in the mice treated with R1-GST. $^{**}P < 0.01$.

obtained from C57BL/6J mice (Jackson Laboratories) to generate chimeric mice, which we then mated with C57BL/6J females. We crossed F1 heterozygotes with C57BL/6J over more than four generations, and then intercrossed them to generate *COL17*$^{m-/-}$ mice.

Screening of *COL17*$^{m-/-}$ mice by PCR, RT-PCR, northern and western blotting, histology, electron microscopic findings and immunofluorescence study. Details of these procedures are in the **Supplementary Methods**.

Generation of rescued *COL17*$^{m-/-,h+}$ COL17-humanized mice. We crossed transgenic mice (C57BL/6 background) expressing the squamous epithelium–specific K14 promoter and a human *COL17 cDNA* (*COL17*$^{m+/+,h+}$) with heterozygous *COL17*$^{m+/-}$ mice. Mice that carried both the heterozygous null mutation of *COL17* and the transgene of human COL17 (*COL17*$^{m+/-,h+}$) were bred to produce rescued *COL17*$^{m-/-,h+}$ COL17-humanized mice.

Table 2 Epitope decoy therapy with COL17 antigenic peptide

	Skin detachment
IgG 1 mg	15/16
IgG 1 mg + GST 800 μg	12/16
IgG 1 mg + R1-GST 600 μg	1/17

The recombinant peptide R1-GST carrying COL17 antigenic sequences markedly suppressed skin detachment in experimental mice injected with BP autoantibodies *in vivo*.

Preparation and characterization of IgG fractions from individuals with BP. We obtained sera from five individuals with BP during the early, active phase of the disease. We performed indirect immunofluorescence (IIF) using normal human skin as a substrate obtained from surgical operations. We defined the IIF titer as the highest dilution of the sera that showed positive fluorescence along the dermal-epidermal junction. We measured the ratio of autoantibody index values in the individuals' sera recognizing COL17 (measured by ELISA using the COL17 NC16A domain peptide) and BP230 using ELISA kits as per the manufacturer's instructions (MBL). We defined the ELISA index value by the following formula: index = (optical density (OD) of tested serum – OD of negative control)/(OD of positive control – OD of negative control) × 100. We prepared the total IgG fractions from these serum samples by affinity chromatography using HiTrap Protein G HP (Amersham Biosciences), and we followed a selection of sera ($n = 3$) by affinity purification directed against entire region of COL17 NC16A domain peptide (R1, amino acids 490–566; see below) using HiTrap NHS-activated HP column (Amersham) as per the manufacturer's instructions. We dialyzed the IgG fractions against PBS and concentrated by ultrafiltration (Millipore).

Passive transfer studies. We performed passive transfer of IgG into mice as described previously with minor modifications[4,5,9]. Briefly, each mouse received a single intraperitoneal injection of IgG (dose: 0.05–2 mg/g body weight). At 48 h after the injection, we judged whether a distinct Nikolsky sign was observed in the skin or not. We then killed the mice and studied the skin samples by light microscopy and direct immunofluorescence microscopy

using FITC-conjugated rat antibody to human IgG (1:100; Jackson Immunoresearch Laboratories).

Generation of recombinant COL17 NC16A peptide. We synthesized 77 amino acids spanning the COL17 NC16A domain (R1, amino acids 490–566) and the 45 amino acids in its N terminus half (R2, amino acids 490–534) as GST-fusion proteins using the expression vector pGEX2-T (Amersham Biosciences) and bacteria BL21 (Amersham Biosciences), as reported previously[10]. In this study, we used both native GST-fusion forms, R1-GST and R2-GST, and GST-cleaved forms (R1 and R2). Other amino acids R3 (amino acids 490–525), R4 (amino acids 490–509), R5 (amino acids 506–525) and R6 (amino acids 526–559) peptides were chemically synthesized (R3 and R6, Greiner Bio-one; R4 and R5, Nippi).

Therapeutic study of COL17 NC16A domain antigenic peptide. Preliminarily *in vitro* immune-adsorption studies showed that a 77–amino acid recombinant peptide (R1) most efficiently suppressed the BP antibody index value from BP sera (see **Fig. 3b** and **Supplementary Methods**). We selected the R1-GST peptide for use in the *in vivo* decoy therapy. For the *in vivo* study, each mouse received a subcutaneous injection of 300 μg of R1-GST fusion protein desalted in 20 mM Tris-HCl, pH 7.5, to the dorsal skin soon after and 24 h after a 1 mg intraperitoneal injection of total IgG from three individuals with BP ($n = 17$). For controls, the same dose of GST was used ($n = 16$).

All mouse procedures were approved by the Institutional Animal Care and Use Committee of Hokkaido University, and full, written informed consent was obtained from all individuals for the use of their human materials.

Statistical analysis and ethical considerations. We examined growth differences between groups for statistical significance using analysis of variance (ANOVA) with Fisher's protected least significant difference (PLSD) test. For therapeutic analysis of the effects of synthetic peptide treatments, we determined statistical significance using the Student's *t*-test. We considered *P* values less than 0.05 as significant.

Note: Supplementary information is available on the Nature Medicine website.

ACKNOWLEDGMENTS

We thank M. Sato, A. Honda, A. Nagasaki and E. Nishizono for technical assistance. This work was supported in part by Grants-in-Aid for Scientific Research from the Japan Society for the Promotion of Science (15390336, 17209038 and 18013002 to H.S.; 17659331, 18390309 and 18659315 to D.S.); by the Project for Realization of Regenerative Medicine from the Ministry of Education, Science, Sports and Culture of Japan (2003–2007 to H.S.); by a grant from the US National Institutes of Health (RO1 AR048982 to K.B.Y.); by a grant from Nu Skin Japan; and by Health and Labour Sciences Research Grants from the Ministry of Health, Labour and Welfare of Japan (2004–2006 to H.S.)

COMPETING INTERESTS STATEMENT

The authors declare that they have no competing financial interests.

Published online at http://www.nature.com/naturemedicine
Reprints and permissions information is available online at http://npg.nature.com/reprintsandpermissions

1. Jacobson, D.L., Gange, S.J., Rose, N.R. & Graham, N.M.H. Epidemiology and estimated population burden of selected autoimmune diseases in the United States. *Clin. Immunol. Immunopathol.* **84**, 223–243 (1997).
2. Taneja, V. & David, C.S. Lessons from animal models for human autoimmune diseases. *Nat. Immunol.* **2**, 781–784 (2001).
3. Gregersen, J.W., Holmes, S. & Fugger, L. Humanized animal models for autoimmune diseases. *Tissue Antigens* **63**, 383–394 (2004).
4. Anhalt, G.J., Labib, R.S., Voorhees, J.J., Beals, T.F. & Diaz, L.A. Induction of pemphigus in neonatal mice by passive transfer of IgG from patients with the disease. *N. Engl. J. Med.* **306**, 1189–1196 (1982).
5. Roscoe, J.T. *et al.* Brazilian pemphigus foliaceus autoantibodies are pathogenic to BALB/c mice by passive transfer. *J. Invest. Dermatol.* **85**, 538–541 (1985).
6. Madsen, L.S. *et al.* A humanized model for multiple sclerosis using HLA-DR2 and T-cell receptor. *Nat. Genet.* **23**, 343–347 (1999).
7. Wen, L. *et al. In vivo* evidence for the contribution of human histocompatibility leukocyte antigen (HLA)-DQ molecules to the development of diabetes. *J. Exp. Med.* **191**, 97–104 (2000).
8. Anhalt, G.J. *et al.* Pathogenic effects of bullous pemphigoid autoantibodies on rabbit corneal epithelium. *J. Clin. Invest.* **68**, 1097–1101 (1981).
9. Liu, Z. *et al.* A passive transfer model of the organ-specific autoimmune disease, bullous pemphigoid, using antibodies generated against the hemidesmosomal antigen, BP180. *J. Clin. Invest.* **92**, 2480–2488 (1993).
10. Zillikens, D. *et al.* Tight clustering of extracellular BP180 epitopes recognized by bullous pemphigoid autoantibodies. *J. Invest. Dermatol.* **109**, 573–579 (1997).
11. McGrath, J.A. *et al.* Mutations in the 180-kD bullous pemphigoid antigen (BPAG2), a hemidesmosomal transmembrane collagen (COL17A1), in generalized atrophic benign epidermolysis bullosa. *Nat. Genet.* **11**, 83–86 (1995).
12. Gatalica, B. *et al.* Cloning of the human type XVII collagen gene (COL17A1), and detection of novel mutations in generalized atrophic benign epidermolysis bullosa. *Am. J. Hum. Genet.* **60**, 352–365 (1997).
13. Shimizu, H. *et al.* The 97 kDa linear IgA bullous dermatosis antigen is not expressed in a patient with generalized atrophic benign epidermolysis bullosa with a novel homozygous G258X mutation in COL17A1. *J. Invest. Dermatol.* **111**, 887–892 (1998).
14. Ishiko, A. *et al.* Human autoantibodies against the 230-kD bullous pemphigoid antigen (BPAG1) bind only to the intracellular domain of the hemidesmosome, whereas those against the 180-kD bullous pemphigoid antigen (BPAG2) bind along the plasma membrane of the hemidesmosome in normal human and swine skin. *J. Clin. Invest.* **91**, 1608–1615 (1993).
15. Zillikens, D. *et al.* Antibodies to desmogleins 1 and 3, but not to BP180, induce blisters in human skin grafted onto SCID mice. *J. Pathol.* **193**, 117–124 (2001).
16. Franzke, C.W., Bruckner, P. & Bruckner-Tuderman, L. Collagenous transmembrane proteins: recent insights into biology and pathology. *J. Biol. Chem.* **280**, 4005–4008 (2005).
17. Laczko, I. *et al.* Conformational consequences of coupling bullous pemphigoid antigen peptides to glutathione-S-transferase and their diagnostic significance. *J. Pept. Sci.* **6**, 378–386 (2000).